Segmental Dynamics in the Crystalline Phase of Nylon 66: Solid-State ^2H NMR†

J. Hirschinger,‡ H. Miura,§ K. H. Gardner, and A. D. English*

Central Research and Development Department, Experimental Station, E. I. du Pont de Nemours and Co., Wilmington, Delaware 19880-0356.
Received August 10, 1989; Revised Manuscript Received October 20, 1989

ABSTRACT: Solid-state deuterium NMR spectroscopy coupled with line-shape simulations has been used to examine the segmental dynamics in selectively deuterated nylon 66 polymers over a wide temperature range. Contributions to the experimental line shape from crystalline and noncrystalline domains may be quantitatively decomposed by employing spin–lattice relaxation time discrimination above −50 °C. N–D and C–D groups in the crystalline domains are found to undergo spatially heterogeneous librational motion (not discrete jumps) both below and above the Brill transition. The N–D groups undergo rapid, but quite restricted, librational motion at all temperatures below the melting point, reflecting the preservation of the hydrogen bonds. The amplitude of motion of the methylene groups in each moiety is very similar, but those located in the adipoyl moiety execute a larger amplitude motion than those located in the hexamethylene diamine moiety at temperatures below the Brill transition. Above the Brill transition, the amplitude of the rapid librational motion of all of the methylene group C–D bonds is quite similar. The mean correlation time of the librational motion is substantially longer for the N–D groups (~300 ps) than for the C–D groups (~40 ps). The motion of the C–D bonds is the same for both dry and wet (2 wt %) polymers. Furthermore, a complete redetermination of the temperature dependence of the X-ray crystal structural parameters has been carried out to facilitate a critical comparison of the experimental structure and the structural requirements of various models of molecular motion.

Introduction

Solid-state NMR methods have been of use in elucidating the dynamics of macromolecules at both the segmental[1] and molecular entanglement length scales.[2,3] At the segmental level, this approach has been used to characterize the rates and amplitudes of motion, with great molecular specificity, of both completely amorphous[4,5] and semicrystalline[6,7] polymers. Our previous contributions to this field have all employed polymers (PTFE,[6] PET,[8] PPDTA,[9] POM,[10] 1,4PB[3]) which have not been specifically synthesized or modified so as to allow the application of various NMR methods; this approach has been followed to assure that the results are indeed representative of the titled polymer and not substantially influenced by the modifications of the structure employed to facilitate application of the NMR methods. The reality of the potential difficulty that can be introduced by the use of specialized synthetic methods, particularly for high molecular weight polymers which have been deuterated, has been illustrated by both calorimetric experiments with polyethylene[11] and neutron-scattering studies of 1,4-polybutadiene.[12] Nevertheless, we have chosen to use specifically deuterated polymers and ^2H NMR methods to probe the segmental dynamics of nylon 66. However, in the present case, where the polymer molecular weight is typical of that found for condensation polymers (which is substantially lower than that found for polyolefins) and the degree of deuteration (less than 20% of the hydrogens has been replaced by deuterium in each polymer) is relatively small, we believe that these results are representative of commercial nylon 66 produced by melt condensation methods.

The experimentally determined mechanics of motion for the polymers that have been previously studied with solid-state NMR methods have been used to test various theoretical models of segmental motion. There exist a considerable number of models for methylene chains,[13,14] but in these cases it is experimentally difficult to identify individual chain sites and characterize the different types of motion that each methylene group and its neighbors undergo. Indeed, it is this very similar chemical nature of adjacent methylene sites in aliphatic polyamides that precludes the use of either solid-state ^1H or ^{13}C NMR methods to quantitatively characterize their chain dynamics; the ^{13}C chemical shift difference between adjacent methylene groups in segments containing at least six carbons is quite small.[15] We present here the results of a solid-state ^2H NMR study of the segmental dynamics of specifically deuterated nylon 66 polymers (polyhexamethylene adipamides). These results allow us to individually identify the molecular motion that each methylene unit and the N–D bonds undergo and thus to examine questions as to the types of motion extant in five- and seven-bond polymethylene segments which are hindered at their termini by the hydrogen-bonding amide sites. Furthermore, these results may afford us the opportunity to gain some qualitative insight as to the cooperativity of motion in this system.

We have previously reported[16] the preparation and characterization of specifically isotopically labeled high molecular weight nylon 66 polymers. The polymers were selectively deuterated in the diamine moiety at the C_1 and C_6 carbons (NY16NHME), the C_2 and C_5 carbons (NY25NHME), and the C_3 and C_4 carbons (NY34NHME) and in the adipoyl moiety at the C_2 and C_5 carbons (NY25COME) and the C_3 and C_4 carbons (NY34COME). After melt equilibration, four of the polymers are labelled only at one chemically unique site and one of the polymers (NY25CO) is partially deuterated both at the intended methylene group and also on the nitrogen (2/3 of the deuterium is bonded to the carbon and 1/3 of the deuterium is bonded to the nitrogen). The molecular weight distribution of these polymers is essentially identical with a most probable distribution as is found

* To whom correspondence should be addressed.
† Contribution No. 5222.
‡ Current address: Max-Planck-Institut fur Polymerforschung, Postfach 3148, D-6500 Mainz, Federal Republic of Germany.
§ Permanent address: Sumitomo Chemical Co., Tsukuba Research Laboratory, 6 Kitahara, Tsukuba, Ibaraki 300-32, Japan.

0024-9297/90/2223-2153$02.50/0

for commercially available polymers prepared via melt condensation polymerization with $M_n \simeq 20\,000$ g/mol. The polymers possess the α crystalline modification[17] and have been characterized as being 35% crystalline by X-ray diffraction and 40% crystalline by DSC methods.[16] Preparation of the polymer labeled at the amide nitrogen (N–D) is reported in the next section.

Experimental Section

^{2}H NMR (30.722 MHz) spectra were obtained with a Bruker MSL-200 NMR spectrometer. Fully relaxed spectra were acquired with a standard quadrupolar echo sequence $((\pi/2)_x - \tau_1 - (\pi/2)_{-y} - DO - (\pi/2)_{-x} - \tau_1 - (\pi/2)_{-y} - DO)$ where the data are acquired during the DO period and alternately added and subtracted. the $\pi/2$ radio-frequency pulse was nominally 2.8 μs in length, the delay time τ_1 was 20 μs in length except in those experiments where it was varied, and the recycle delay time, DO, was varied so that it was at least equal to 5 times the spin–lattice relaxation time of the slowest relaxing component in the spectrum. The $\pi/2$ pulse width was sufficiently short to allow spectral acquisition with minimal spectral distortion.[18] Data (4096 points) were acquired at a rate of 2 MHz and then shifted to the top of the spin echo prior to Fourier transformation. The probe was carefully tuned following the multiple pulse tuning procedure of Gerstein[19] at all temperatures, using a sample of liquid acetone-d_6 at low temperatures and a sample of liquid D_2SO_4 at high temperatures, to minimize spectral distortion.[20-22] The tuning procedure used 60 pulses of duration 2.8 μs each separated by 170 μs. The temperature was controlled with a Bruker B-VT 1000 unit over the range −180 to 230 °C and was calibrated with a digital thermometer with a thermocouple that had been placed coaxially inside an NMR tube packed with polymer in the NMR probe.

Spin–lattice relaxation times (T_1) were measured over the same temperature range used to acquire the fully relaxed spectra employing a saturation recovery method. The pulse sequence used was $((\pi/2)_x - t)_9 - (\pi/2)_x - \tau_0 - (\pi/2)_x - \tau_1 - (\pi/2)_{-y} - DO - ((\pi/2)_{-x} - t)_9 - (\pi/2)_{-x} - \tau_0 - (\pi/2)_{-x} - \tau_1 - (\pi/2)_{-y} - DO$, where t has a value of 3 ms, τ_0 is varied from 5 ms to 60 s, τ_1 has a value of 20 μs, and again the data are alternately added and subtracted. Values of T_1 were calculated from the evolution of the total magnetization as a function of τ_0 in the time domain; these data were fit in a least-squares sense to a sum of two or more exponential decays. Details of the fitting procedure are given in Appendix A. The same pulse sequence was used to obtain partially relaxed spectra (τ_0 = 5 times the shorter spin–lattice relaxation time); furthermore, these spectra were subtracted from the fully relaxed spectra to obtain spectra of those spins with the longest spin–lattice relaxation time.

Spin alignment relaxation times (T_{1Q}) were measured at selected elevated temperatures. The pulse sequence used was $(\pi/2)_x - \tau_1 - (\pi/4)_{-y} - \tau_2 - (\pi/4)_{-y} - \tau_1 - DO - (\pi/2)_{-x} - \tau_1 - (\pi/4)_{-y} - \tau_2 - (\pi/4)_{-y} - \tau_1 - DO$,[23] where τ_1 has a value of 20 μs, τ_2 is varied from 5 ms to 60 s, and once again the data are alternately added and subtracted. T_{1Q}-distorted line shapes of only those spins with the longer relaxation time were obtained directly by adjusting the value of τ_2 to be much longer than the shortest T_{1Q} value.

Variable-temperature (25–250 °C) X-ray diffraction patterns of melt-recrystallized nylon 66 were obtained by using a Rigaku Θ–Θ diffractometer run in the horizontal mode (Cu Kα radiation). Digital data were collected in a fixed time mode at intervals of 0.02° in 2Θ. The 2Θ scale was calibrated with silicon (NBS-640A) as an internal standard, and the temperature was measured by a thermocouple embedded in the sample. Background scattering in the diffraction patterns was fitted with a cubic spline function and removed. The remaining pattern was fit with a series of Gaussian peaks that were defined by the refinable parameters of height, width, and position. The peak positions were corrected for distortions and change in sample height (thermal expansion) by using the experimentally determined positions of five silicon peaks and the known thermal expansion of silicon.

Nylon 66 polymer selectively deuterated at the amide nitrogen was prepared by dissolution of Zytel 101 nylon 66 polymer in HCOOD at 10 wt % at ~50 °C. The solution was stirred for 16 h, precipitated in D_2O with stirring in a blender, and then filtered through a sintered glass filter. The polymer was then washed in a blender with D_2O and filtered 9 more times to ensure neutrality prior to drying in a vacuum oven at 100 °C with a N_2 purge for 16 h. The polymer was sealed under vacuum in a 5-mm NMR tube for future use. Analysis of the extent of deuteration of the N–D site in this polymer by diffuse reflectance infrared spectroscopy indicated that the polymer was 75% deuterated, and solid-state ^{2}H NMR indicated the polymer was 71% deuterated.

Preparation of nylon 66 polymer with 2% ± 0.3% water is described in the following paper in this issue.

^{2}H NMR Line-Shape Simulations and Models of Motion

Due to the large magnitude of the quadrupolar coupling constant (ν_Q = 100–200 kHz), the free induction decay (FID) following a 90° pulse is very rapid (a few microseconds), so a significant part of the signal is lost during the receiver dead time. Pulsed NMR methods can be used[24] to generate a "solid echo" with two 90° quadrature radio-frequency pulses separated by a time τ_1. The solid echo decay at times $t > 2\tau_1$ is equivalent to the FID for a spin I = 1 experiencing an effectively static coupling. However, when the rate of the molecular motion ν_c is comparable to ν_Q, transverse relaxation (T_2) effects resulting from the fluctuations of the quadrupolar interaction are very important, and, as a result of the orientational dependence of T_2, the solid echo decay is severely distorted as compared to the FID.[25,26] The echo distortion effect can nevertheless be turned into an advantage by providing an additional parameter for studying dynamic processes because the τ_1 dependence is very sensitive to details of the dynamic process.[26-29] Different molecular motions producing identical undistorted spectra may be distinguished on the basis of their τ_1 dependence.[29,30] Moreover, very restricted motions which lead to only minor averaging of the quadrupolar interaction can be easily detected by the T_2 relaxation. The extensive study of T_2 distortions is then expected to be especially useful in disordered systems like amorphous polymers, where, as a consequence of the heterogeneity of the structure, broad inhomogeneous distributions of both rates[30,31] and amplitudes[3-6,8,10,32,33] of the motion lead to very unspecific undistorted line shapes (see below). Additionally, complementary information can be obtained from the spin–lattice relaxation, which is sensitive to molecular motion near the Larmor frequency.[28,34]

Line-Shape Simulations: Fast-Motion Limit

When the rate of the motion (ν_c) is much larger than the quadrupolar coupling constant ($\nu_Q = e^2qQ/h$), a specific molecular motion leads to a partially averaged electric field gradient tensor (FGT) defined by an averaged coupling constant (ν_Q*) and an averaged asymmetry parameter (η*). For the case of an axially symmetric static FGT (η = 0, such as a deuterium bonded to an aliphatic carbon) which undergoes rapid uniaxial motion, the line shape depends only on the polar angle (β) and the time-averaged azimuthal distribution ($P(\psi)$) defining the orientations of the unique principal axis (V_3) in the molecular frame.[28] Line-shape simulations are then easily performed for any type of motion.[34] Of course, when the static FGT is not axially symmetric ($\eta \neq 0$, such as a deuterium bonded to a nitrogen), the Euler angle specifying the orientation of the static FGT about V_3 is required, and the expression for the orientational dependence of the resonance frequency is modified.[35] In this paper, three

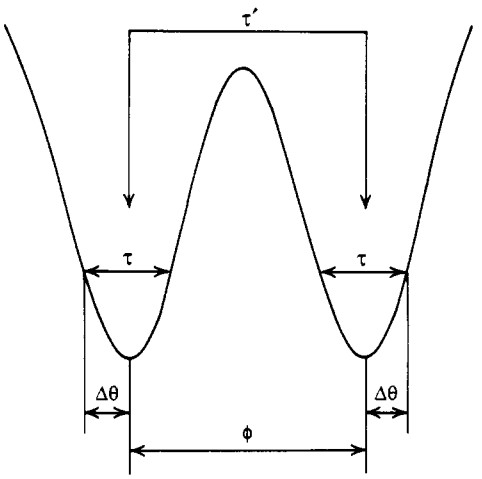

Figure 1. Schematic potential energy diagram for the two-site model used to simulate experimental line shapes. The librational motion is characterized by a characteristic lifetime τ (defined in text) and a Gaussian distribution of angles of standard deviation $\Delta\theta$. The internal rotation motion is characterized by an angle ϕ, with a residence time τ'.

different forms for $P(\psi)$ are considered. The first is a discrete two-site jump where $P(\psi)$ is simply described by the azimuthal jump angle conveniently called ϕ and the site populations P_1 and P_2. Because the vectors defining the orientations of the two sites are always contained in the same plane, we use the jump angle 2β (with $\phi_1 = 0°$ and $\phi_2 = 180°$). The second form is a fast uniaxial libration described by a Gaussian azimuthal distribution $P(\theta)$ of standard deviation $\Delta\theta$ (ψ is conveniently called θ in the case of a Gaussian libration motion). $P(\theta)$ is assumed to be Gaussian because this distribution is an accurate representation of the Boltzmann distribution of angles that a librating bond will sample in the harmonic oscillator limit (Appendix B). The third form is rapid uniaxial restricted diffusion in the angular range $\pm\psi_l$, where $P(\psi) = 1/(2\psi_l)$ between the two limiting values $-\psi_l$ and $+\psi_l$, and $P(\psi) = 0$ outside this interval.[28,36] Unfortunately, because the fast-motion limit line shape only depends on two moments of $P(\psi)$, $\langle\cos\psi\rangle$ and $\langle\cos 2\psi\rangle$,[28] in some cases similar results can be obtained for all of these models of motion, and other information must be known in order to distinguish between these motional mechanisms.[28,34] Small deviations from pure uniaxial libration have been simulated by introducing an additional Gaussian distribution of the polar angle β (standard deviation $\Delta\beta$).

Line-Shape Simulations: Intermediate Exchange

Intermediate-exchange line-shape simulations were performed by using the multisite exchange model originally developed by Wemmer.[37] This calculation gives a zero-delay ($\tau_1 = 0$) or continuous-wave line shape which must be corrected for echo distortions.[25-27] In our simulations, only intermediate-exchange calculations between two equally populated sites appeared to be necessary ($P_1 = P_2$). However, each of the sites was allowed to undergo a fast librational motion in addition to the two-site jump using the so-called sequential method.[38] Once again, we distinguish between the azimuthal jump angle ϕ between the two sites and the azimuthal librational angle θ within each well (Figure 1). The calculation is performed as follows: for each orientation of the static magnetic field H_0, a series of 30–50 isochromats corresponding to a Gaussian distribution $P(\theta)$ of 30–50 azimuthal angles θ (standard deviation $\Delta\theta$) is generated for each well. The 30–50 isochromats are averaged with a population-weighted basis over $P(\theta)$ to yield an isochromat which reflects the rapid librational motion within each well. The resulting two spin isochromats are then allowed to exchange with a residence time in each site τ', and the line shape is corrected for the delay between the quadrature pulses by using the correction factor $K(2\tau_1)$ from the exact theory.[25] This procedure is repeated for 1° steps in both the polar and azimuthal angles of H_0 in the molecular frame to yield a powder pattern. For small values of $\Delta\theta$ (<30°), the unique effect of the fast librational motion is to slightly reduce the breadth of the two-site jump calculation.[28] The correlation time τ_c in s/rad of the jump is related to the residence time in s/cycle by $\tau_c = \tau'/(4\pi)$. We define the correlation frequency (in Hz) as $\nu_c = (2\pi\tau_c)^{-1}$. A simple variation of this model allows the calculation of the effect of a fluctuation between two fast librational states by taking the same coordinates for the two site orientations 1 and 2 ($\phi = 0$) with different standard deviations of libration ($\Delta\theta_1$ and $\Delta\theta_2$). Figure 2 shows the results for a residence time $\tau' = 10^{-5}$ s/cycle in each librational state. Of course, if $\Delta\theta_1 = \Delta\theta_2 = \Delta\theta$, we obtain the line shape due to a simple fast Gaussian libration (see above).

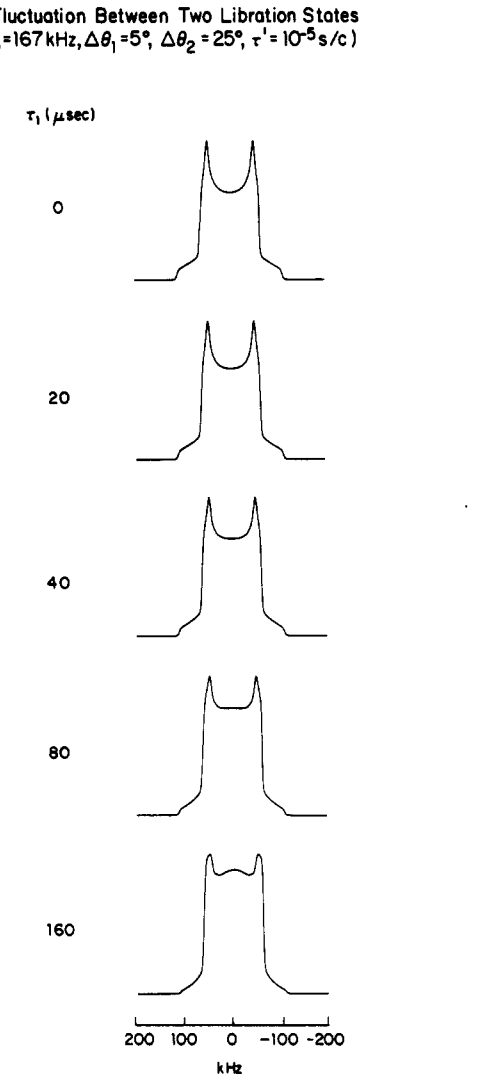

Figure 2. T_2 echo-distorted line shapes for a model of fluctuation ($\tau' = 10^{-5}$ s/cycle) between two librational states, both of which are centered at the same mean value but with different widths ($\Delta\theta_1 = 5°$ and $\Delta\theta_2 = 25°$).

Alternatively, Vega[26] has shown that echo-distorted line shapes can be calculated by using relaxation theory. This method has been used to simulate line shapes for both a

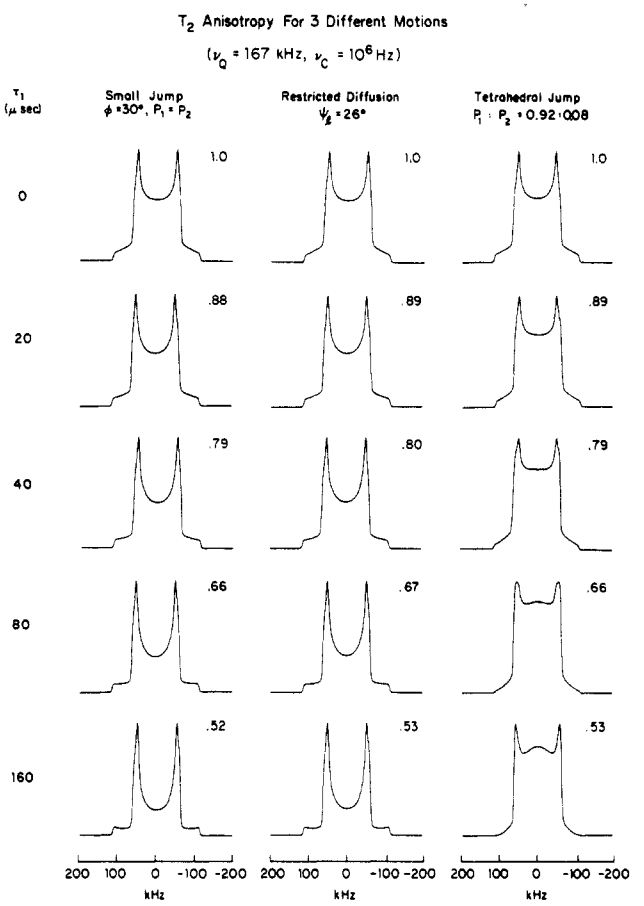

Figure 3. Echo-distorted line shapes for three different motions about a tetrahedral axis ($\beta = 109.5°$). $\nu_c = 10^6$ Hz is defined as $(2\pi\tau_c)^{-1}$. In the case of the jump motions, $(\tau_c)^{-1}$ is equal to the sum of the rate constants $(k_{12} + k_{21})$ for jumping from one site to the other. In the case of the restricted diffusion, $\tau_c = 4\psi_l^2/(D_i\pi^2)$ with D_i the internal diffusion coefficient defined in ref 27. The line shapes in the left column are those calculated for an equal population jump over an angle of 30°. The line shapes in the middle column are those calculated for a model of restricted uniaxial diffusion over the angular range ±26°. The line shapes in the right column are those calculated for a model of a tetrahedral jump where the populations of the two sites are in the ratio 92/8. Numbers next to each line shape are the integrated reduction factors.

two-site jump model with unequal populations and a model of uniaxial diffusion restricted between two limiting azimuthal angles $\pm\psi_l$. If the correlation time of the motion τ_c is much smaller than τ_1, the orientation-dependent correction factor $K(2\tau_1)$ is equal to $\exp(-2\tau_1/T_2)$. In this limit, T_2 is given by simple relaxation theory in the weak collision limit[35] as $1/T_2 = 2\pi^2\nu_Q^2 J_0(0)$, neglecting the nonsecular terms with $\eta = 0$. $J_0(0)$ can be calculated for various jump and diffusive models of motion by using the general formalism of ref 39. For each orientation of H_0, the two isochromats can then simply be averaged over $P(\psi)$, and the line shape is multiplied by $K(2\tau_1)$.

Figure 3 shows echo-distorted line shapes for three different restricted motional processes utilizing this formalism. For a correlation time of $\tau_c = 1.6 \times 10^{-7}$ s/rad, the $\tau_1 = 0$ line shapes for all three models are indistinguishable; i.e., exchange broadening is negligible (fast-exchange limit). However, the T_2 echo distortions are vastly different even for these relatively short τ_1 delays used here. (The most prominent features of the echo-distorted line shapes are determined by those isochromats which are in the fast-exchange limit.) Figure 3 shows that when $\tau_c > 10^{-8}$ s/rad the relative echo distortions observed in the central portion of the line shapes of a tetrahedral ($2\beta = 109.5°$) two-site jump with $P_1 \gg P_2$ model are relatively smaller at long τ_1 as compared to the line shapes of a small-angle jump model. More generally, we have verified that these characteristic T_2 distortions allow differentiation of large-angle two-site jumps ($60° < 2\beta < 120°$, $P_1 \gg P_2$) from small-angle equal population jumps ($2\beta < 30°$, $P_1 = P_2$). On the other hand, it appears that it is impossible to differentiate restricted diffusion ($\psi_l^2 \ll 1$) from small-angle jumps ($P_1 = P_2$). Thus, it can be concluded that fast small-angle fluctuations within a plane (jump-like or diffusive) are generally characterized by intensity losses in the central region of the Pake-like powder pattern; hence, so long as $\tau_c \ll \tau_1$ and $60° < \beta > 120°$, a two-site jump ($P_1 = P_2$) of azimuthal angle $\phi = 2\Delta\psi$ constitutes a very good approximation for small-angle fluctuation (jump-like or diffusive) with a time-averaged distribution $P(\psi)$ of standard deviation $\Delta\psi$ ($\Delta\psi^2 \ll 1$). The characteristic lifetime (τ) of the small-angle fluctuation is defined as the residence time (s/cycle) of the equivalent two-site jump ($P_1 = P_2$, $\phi = 2\Delta\theta$). (When $P(\psi)$ is rectangular (restricted diffusion), $\Delta\psi = \psi_l/(3^{1/2})$.) These results illustrate that anisotropic T_2 relaxation significantly expands our ability to differentiate models of motion with fast correlation times. Unfortunately, this method is limited to $\tau_c > 10^{-8}$ s/rad because the static nuclear dipolar interactions, characterized by a transverse relaxation time $T_{2d} < 500$ μs, dominate the spin–spin relaxation for smaller values of τ_c.[30] This problem can be overcome by employing the anisotropy of the spin–lattice relaxation.[28,34,39]

In the limit of $\tau_c \ll \tau_1$, differentiation between a two-site jump ($P_1 = P_2$) and restricted diffusion ($\beta = 109.5°$) is also effectively impossible for larger diffusion amplitudes ψ_l and jump angles 2β, because significant differences in the line shapes are only observed in the calculations at very long τ_1 values where the signal intensity is so small (T_2 dipolar relaxation) as to be experimentally intractable. A distinction between these two motional mechanisms is predicted in the intermediate- and slow-motion limit ($\tau_c \geq \tau_1$) where the relaxation strongly depends on the details of the motion.[26] The spin–spin relaxation is nevertheless still dominated by the nonselective dipolar interactions when $\tau_c \gg T_{2d}$. As shown by Spiess,[23] ultraslow motions can still be studied by using the Jeener–Broekart three-pulse sequence for $\tau_c < T_{1Q}$ where the spin–lattice relaxation time of the deuteron spin alignment (T_{1Q}) is generally longer than 10 ms. Another drawback of the solid echo method lies in the fact that T_2 becomes quite short when $\tau_c \simeq \tau_1$ so that the echo intensity is very weak, especially when the motion tends to sample many different orientations.[25,26,28,40] Figure 4 shows the theoretical integrated reduction factor of the powder spectrum (amplitude of the solid echo at $t = 2\tau_1$) for a two-site jump motion ($P_1 = P_2$) as a function of $1/\tau'$ for different jump angles 2β. It is seen that, even for this highly spatially restricted motion, the fraction of magnetization refocused at a short delay ($\tau_1 = 20$ μs) can be as low as 22% when the jump angle is close to 90°. Note that the residual magnetization, under these typical experimental conditions, is not essentially zero (contrary to popular belief).

Line-Shape Simulations: Corrections

The calculated powder patterns are corrected for finite pulse length[18] and convoluted with Gaussian and Lorentzian broadenings. No corrections to the calculated line shapes due to molecular motion during the radio-frequency pulses were attempted.[41] The simulations use a Gaussian broadening, determined from the low-

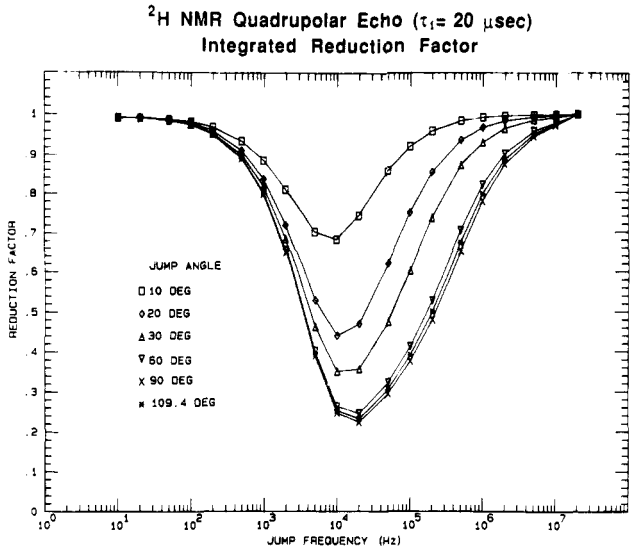

Figure 4. Theoretical integrated reduction factor of the powder spectrum (amplitude at the top of solid echo) for a two-site jump motion ($P_1 = P_2$) as the function of jump frequency $1/\tau'$ for different jump angles (2β) with a delay between quadrature pulses of 20 μs.

Table I
Gaussian Broadening (kHz) in Slow-Exchange Powder Patterns

polymer	noncrystalline	crystalline
NY16NHME	2.2	2.5
MY25NHME	1.5	2.0
NY34NHME	1.2	1.6
NY25COME	2.2	2.5
NY34COME	1.7	2.2

temperature spectra, to account for dipolar interactions to both ^{2}H and ^{1}H neighboring nuclei. This broadening is in the range 1.2–2.5 kHz (see Table I) and is reasonable when compared with that used previously for fully deuterated polyethylene (1.3 kHz) and model compounds.[42,43] Previous reports[44] of the interpretation of ^{2}H NMR line shapes in selectively labeled poly(butyleneterephthalate) have evidently used a Gaussian broadening near 10 kHz in their simulations and thus are unlikely to be able to differentiate some of the models of motion discussed here. The Lorentzian broadening is determined by that used in the processing of the experimental data (1-kHz full width at half-maximum). Figure 5 illustrates a ^{2}H NMR spectrum of hexanedioic acid-2,2,-5,5-d_4 obtained at 23 °C and a calculated spectrum which uses a Gaussian broadening of 1.4 kHz and a Lorentzian broadening of 1 kHz; the best fit to this spectrum was obtained by using a $\pi/2$ pulse length of 3.2 μs. This apparent lengthening of the effective pulse length from the 2.8 μs used in the pulse programmer is a manifestation of the nonpurely resistive load characteristics of the probe. All subsequent simulations were carried out using a $\pi/2$ pulse length of 3.2 μs.

Line-Shape Simulations: Inhomogeneous Distributions

In the fast-motion limit, a spatially unique molecular motion is described by a single distribution $P(\psi)$ and thus leads to a well-defined powder pattern completely characterized by ν_Q^* and η^*. ν_Q^* and η^* are directly related to the singularities of the powder pattern. However, we observe line shapes which show no T_2 distortion and also do not feature any well-defined singularities. The fact that no T_2 distortion is observed implies that the relaxation is entirely controlled by the nonselective static dipolar interactions. Considering only a distribution of correlation times and one trajectory of motion, this case ($T_2 = T_{2d}$) will be observed only if the motion is either very slow, very fast, or if the distribution of correlation times is so large that the intermediate-exchange line shapes are unobservable due to both a minimal population and fast T_2 relaxation.[45] These three cases will result, respectively, in a slow-motion-limit spectrum defined by ν_Q and η, a fast-motion-limit spectrum defined by ν_Q^* and η^*, or a weighted sum of these two well-defined line shapes. Clearly, even in the latter case, singularities must be observed. Because the experimental results do not show evidence of any singularities (see below and following paper), the motion extant in this system cannot be described with a single trajectory of motion, and thus an inhomogeneous distribution of amplitudes of motion has to be considered. Distributions of both jump angles ($P(\phi)$) and librations ($P(\Delta\theta)$) were then introduced by simply calculating the population-weighted summation of the line shapes according to the inhomogeneous distribution ($P(\phi)$ or $P(\Delta\theta)$). Good agreement with the experimental data is then obtained with no need for a distribution of correlation times.

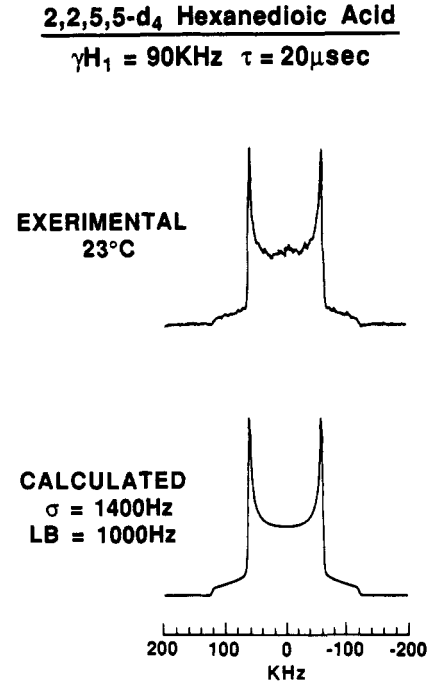

Figure 5. Experimental and calculated ^{2}H NMR spectra of hexanedioic acid-2,2,5,5-d_4. The molecule is assumed to be rigid, and a Gaussian broadening of 1.4 kHz, a Lorentzian broadening of 1 kHz, and an effective $\pi/2$ pulse length of 3.2 μs were used in the simulation.

Results and Discussion

Spin–Lattice Relaxation Discrimination of Magnetization from Crystalline Domains. Assignment of magnetization to either crystalline or noncrystalline domains is critically dependent upon the ability of some experiment to differentiate magnetization arising from each of these domains. Figure 6 illustrates the temperature dependence of the fractional magnetization of a two-component fit of the saturation recovery spin–lattice relaxation time measurement for one of the selectively deuterated nylon 66 polymers (NY16NHME). It is clear that at lower temperatures there is some mixing, even in this simple two-phase model, due to some fraction of the amorphous material giving rise to magnetiza-

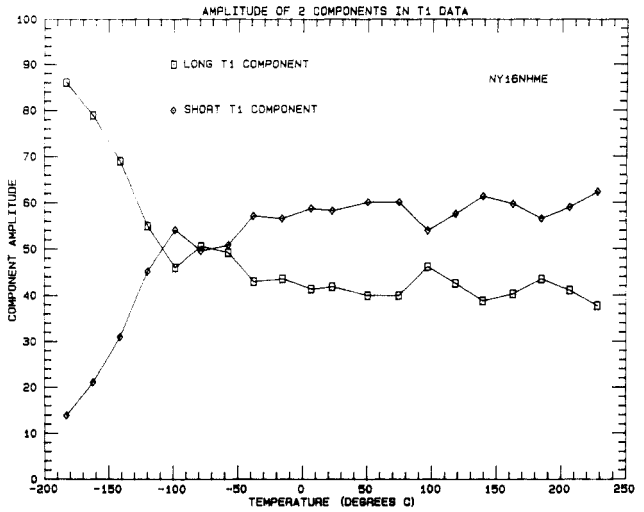

Figure 6. Relative amplitudes of magnetization in a two-component fit of spin–lattice relaxation time data from a saturation recovery curve as a function of temperature for the polymer NY16NHME. The open squares are due to the long-T_1 component, and the open diamonds are for the short-T_1 component.

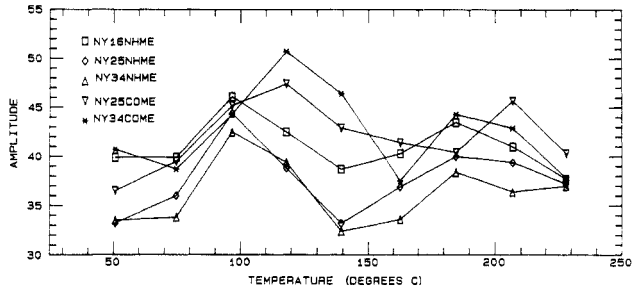

Figure 7. Amplitude of magnetization associated with the long-T_1 component for each of the nylon polymers with deuterated methylene groups as a function of temperature.

tion whose spin–lattice relaxation time is quite similar to that arising from the crystalline domains. It is apparent that at temperatures above ~ −50 °C the magnetization appears to be divisible into two components of amplitude of approximately 40% and 60%. Figure 7 shows the temperature dependence of the fraction of magnetization associated with the longer T_1 component for all five selectively deuterated nylons labeled on the methylene groups; it is apparent that this fraction is near 40% ± 10% over the entire temperature range 50–230 °C, and this value compares well with that found for percent crystallinity via X-ray diffraction (35%) and DSC (39%).[16] This component has much longer relaxation times—by factors in the range 24–100 times longer—at all temperatures (Figures 8 and 9) than the other component and thus is associated with magnetization arising from crystalline domains. Attempts to fit the magnetization, at temperatures above −50 °C, to more than two components gave only slightly better statistical fits; thus, it seemed appropriate as a first approximation to use a two-phase model for the spin–lattice-discriminated data. Note that any model of motion describing the line shapes arising from the longer spin–lattice relaxation time component (crystalline domains) requires the use of substantial dynamic heterogeneity (see below); moreover, the shorter spin–lattice relaxation time component (noncrystalline domain) line shapes require the use of models which consider two populations, each of which is characterized by considerable dynamic heterogeneity (see following paper). Thus, it appears that above −50 °C there is sufficient motion (although quite heterogeneous) near the

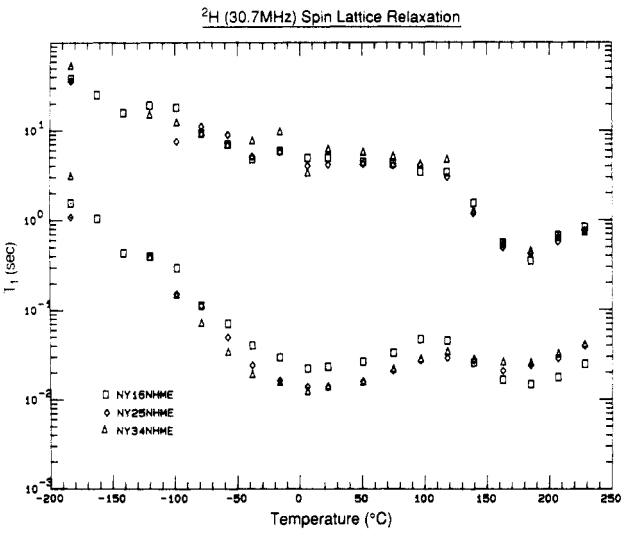

Figure 8. Temperature dependence of spin–lattice relaxation times for the two components of magnetization in a saturation recovery experiment for NY16NHME, NY25NHME, and NY34NHME.

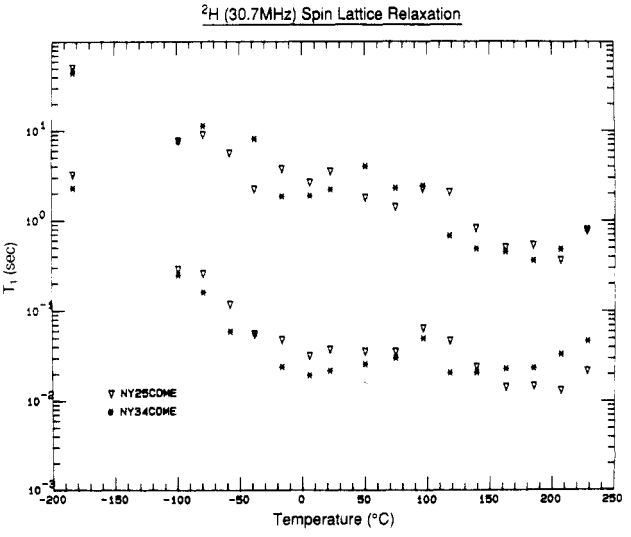

Figure 9. Temperature dependence of spin–lattice relaxation times for the two components of magnetization in a saturation recovery experiment for NY25COME and NY34COME.

Larmor frequency, in the noncrystalline domain, to cause virtually all magnetization from these regions to have a short spin–lattice relaxation time; in contrast, the motion in the crystalline domains may be characterized as heterogeneous, very rapid (compared to the Larmor frequency) small-angle fluctuations whose amplitude grows with temperature (see below), and this motion never leads to rapid spin–lattice relaxation.

Analysis of the data from the N–D polymer indicates that T_1 discrimination is reasonably effective for this polymer also, yielding two components of magnetization each of which is 50% ± 10% above −50 °C.

N–D Motion. In order to limit the number of possible models of motion which must be considered for the methylene groups, the mobility of the N–D bonds was considered first. The mobility of the N–D bond is expected to be greatly constrained by the presence of hydrogen bonding between the carbonyl oxygen and the N–D.[46] The experimental line shapes (Figure 10) illustrate that only a minor amount of motional averaging takes place up to the highest temperature examined (228 °C). Below 180 °C, the line shapes are nicely fitted by a "rigid lattice" simulation with η = 0.17 and ν_Q = 191 kHz. Above

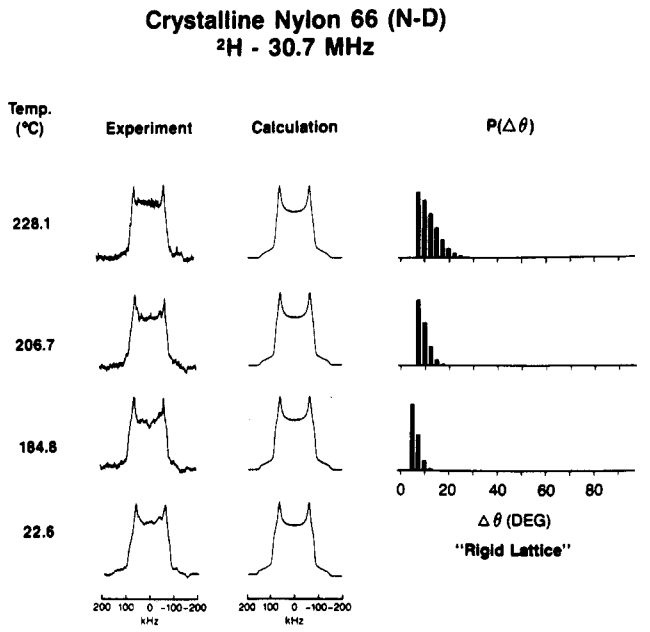

Figure 10. Experimental and calculated ^2H NMR line shapes with the distribution of standard deviations of Gaussian librations used in the calculations for the long-T_1 component (crystalline fraction) of N-D nylon 66.

180 °C, an inhomogeneous distribution of small librational motion about the N–C axis accounts very well for the observed changes in the experimental spectra. The distribution of librations is described by an inhomogeneous distribution of standard deviations of Gaussian librations whose form is illustrated in the right-hand side of Figure 10. The orientation of the static FGT determined for collagen[47] has been used in these simulations with $|V_3| > |V_2| > |V_1|$. V_2 is appreciably averaged by the motion so that the vertical edges of the line shape are smeared out by the inhomogeneous distribution. In contrast, the position of the peaks defined by $V_1^* \simeq V_1$ is not significantly affected by the motion. Because the N–C axis is only 30° from the V_1 axis, libration around the N–C axis provides a good fit to the experimental data. As expected, similar agreement may be obtained for libration about the chain axis itself (i.e., when the libration axis is coincident with V_1). As shown in Appendix D, it is possible to determine a mean correlation time of libration (τ_c) by correlating the line-shape analysis with the spin–lattice relaxation data. This procedure produces values of $2\pi\tau_c$ which vary from 500 to 200 psec over the temperature range 185–228 °C. This value for the rate of the motion clearly justifies the use of a motional model where the rate of the motion is chosen to be much larger than $\nu_Q \sim 10^5$ Hz.

C–D Motion. Figures 11 and 13–16 illustrate the experimental and calculated line shapes and $P(\Delta\theta)$ distributions for each methylene-labeled polymer. The data indicate that there is much more motional averaging for the C–D sites than for the N–D sites. Additionally, it is apparent that the components of the FGT are not easily identified as the temperature is increased because the motion smears out the singularities in the line shapes. At the highest temperature, the spectrum is so featureless that none of the components of the FGT can be determined. This indicates that all of the C–D bonds are not undergoing the same spatially well-defined mode of motion—e.g., the motion is *spatially inhomogeneous*. This conclusion is in consonance with the small average length of crystallite stems of 86 Å,[16] which is approximately five repeat units.

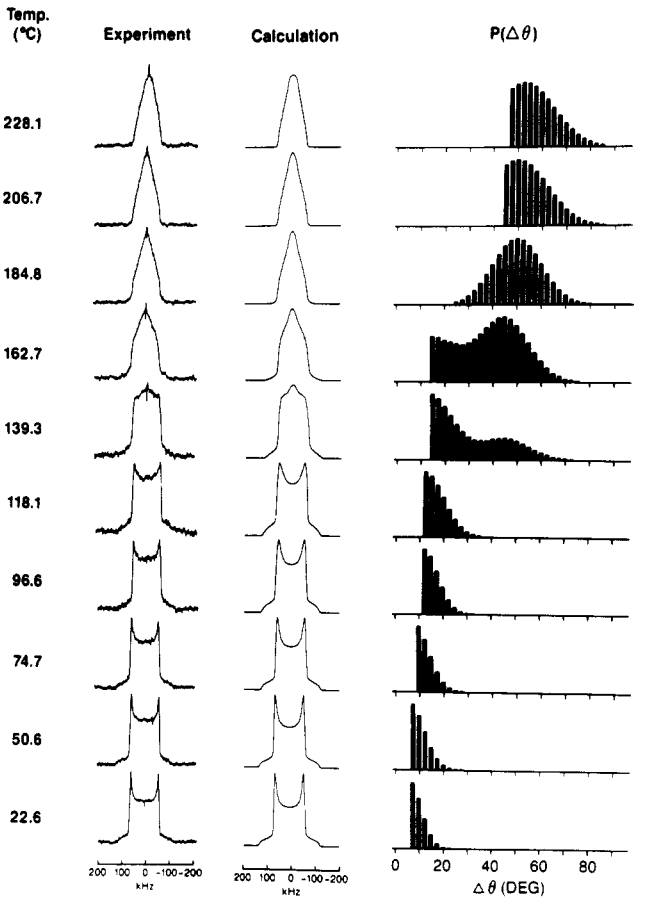

Figure 11. Experimental and calculated ^2H NMR line shapes with the distribution of standard deviations of Gaussian librations used in the calculations for the long-T_1 component (crystalline fraction) of NY16NHME.

At room temperature, the crystalline chains are known to be in the fully extended all-trans conformation,[46] or nearly so,[48] with the segments linked by hydrogen bonds between the C=O and N–H groups to form sheets. As the temperature is increased, the crystalline phase of the polymer undergoes a gradual structural transition (Brill transition) from a triclinic unit cell to a different triclinic (pseudohexagonal) form.[49] From the results (above) concerning the very minor amount of rotational motion present for the N–D groups, the amide groups must be nearly rigid in the hydrogen-bonded sheets so that the remaining degrees of freedom of the main chain atoms consist only of motion about the C–C bonds of the methylene groups; additionally, any such motion must occur in such a way that the amide groups do not rotate. The experimental spectra of Figures 11 and 13–16 are reflective of this motion, and several qualitative conclusions may be drawn about the nature of the motion just from examination of the experimental data. The line shapes at each temperature are essentially identical for the deuterated methylene groups within each moiety; additionally, above ~160 °C the line shapes of all five types of methylene groups appear to be very similar. Below ~160 °C, the line shapes of the methylene groups located in the hexamethylenediamine (HMDA) moiety are characteristic of less motional averaging than the line shapes of the methylene groups located in the adipoyl moiety. (Note that the line shape of NY25COME has a contribution from the N–D line shape due to isotopic scrambling during melt equilibration; however, this poses only

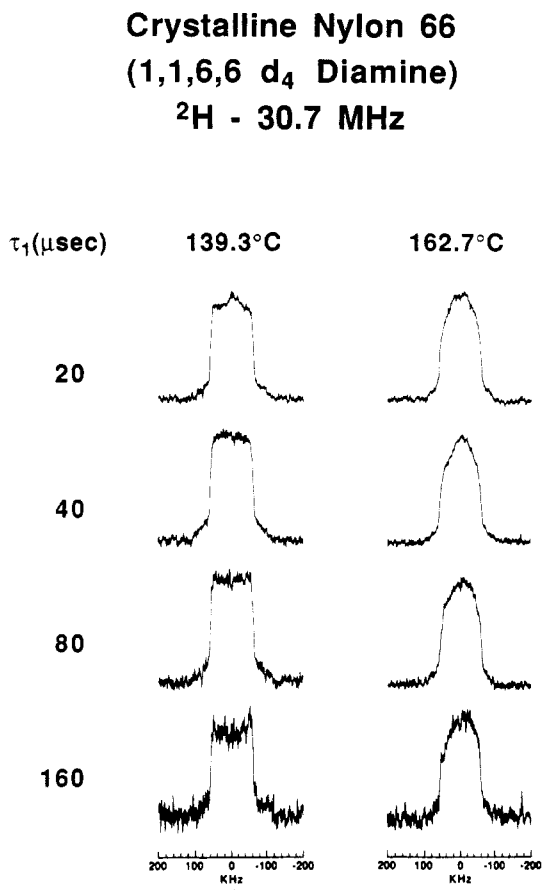

Figure 12. Experimental ^2H NMR line shapes for the long-T_1 component (crystalline fraction) of NY16NHME as a function of delay time (τ_1) for two selected temperatures.

a very minor problem as the N–D line shape is known (see above) and has such a weak temperature dependence that it is easily accounted for in the simulations.) These qualitative observations indicate that the motions of individual methylene groups within each moiety are quite similar at all temperatures and that below 160 °C the motions of the methylene groups in the longer moiety (HMDA) are hindered relative to methylene groups in the shorter moiety (adipoyl). This latter finding is counterintuitive and illustrates the difficulty of making a priori predictions as to the qualitative, let alone quantitative, nature of segmental motion.

Above ~160 °C, the line shapes for all of the methylene groups appear to be close to $\eta^* = 1$ fast-exchange line shapes, which could be interpreted as being indicative of a fast jump motion between two equally populated sites.[25,30,44] This model is only one particular case of a family of two-site jumps which leads to this particular line shape,[34] but is commonly used to model trans–gauche conformational isomerizations. (It is noteworthy that an additional librational motion in each site of the two-site jump must be considered to reduce the magnitude of the splitting between the perpendicular singularities to the observed values of 110–115 kHz from the 125 kHz, which would be observed from a simple two-site jump.) Use of such a two-site jump model requires the creation of gauche conformers; additionally, in order to preserve the linearity of the crystalline chains, each gauche(+) conformer must be compensated with a gauche(−) conformer. The well-known tgtg′ sequence satisfies this requirement and yields the least shortening of the repeat unit length.[50–54] This sequence, with some cooperativity, may diffuse along a chain by a three-bond crank shaft motion[50] and thus provide a mechanism for

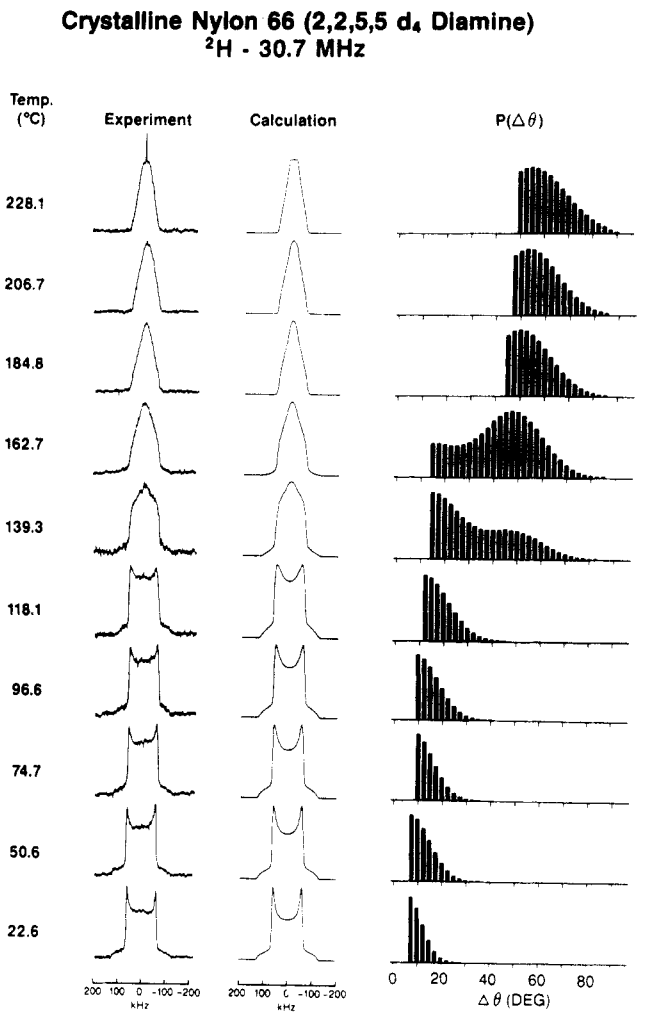

Figure 13. Experimental and calculated ^2H NMR line shapes with the distribution of standard deviations of Gaussian librations used in the calculations for the long-T_1 component (crystalline fraction) of NY25NHME. At the three highest temperatures, a biaxial librational model has been used where the mean value of the second librational distribution at each temperature is 5.6° (184.8 °C), 7.3° (206.7 °C), and 7.7° (228.1 °C).

two-site jumps.[51] In order for this model to be consistent with the experimental data, approximately equal populations of gauche and trans conformers must exist. This requires that a minimum of two tgtg′ sequences exist per repeat unit with one in each of the moieties. Each tgtg′ sequence (unstrained) has been calculated to shorten the chain axis by about 1 Å. Experimental determination of the temperature dependence of the chain axis contraction from room temperature to 170 °C is in the range 0–1 Å (Appendix C) and is apparently quite dependent on the mode of sample preparation.[48,55,56] Thus, the experimentally observed chain axis contraction is much too small to account for the shortening that would be introduced by the introduction of two tgtg′ sequences. Additionally, the fact that the crystallographic changes occur continuously as a function of temperature[55,56] is not consistent with the requirements of the two-site model, which would require a structural transition to introduce a minimum of two tgtg′ sequences into every repeat unit simultaneously. There are also two other problems with this model. First, the tgtg′ sequences cannot be crystallographic "defects" or "kinks"[52] because of their concentration. Also, tgtg′ sequences which are strained to bring the stems back into crystallographic register have considerable energies (~7 kcal/mol), and thus the populations would be quite small at the temperatures employed

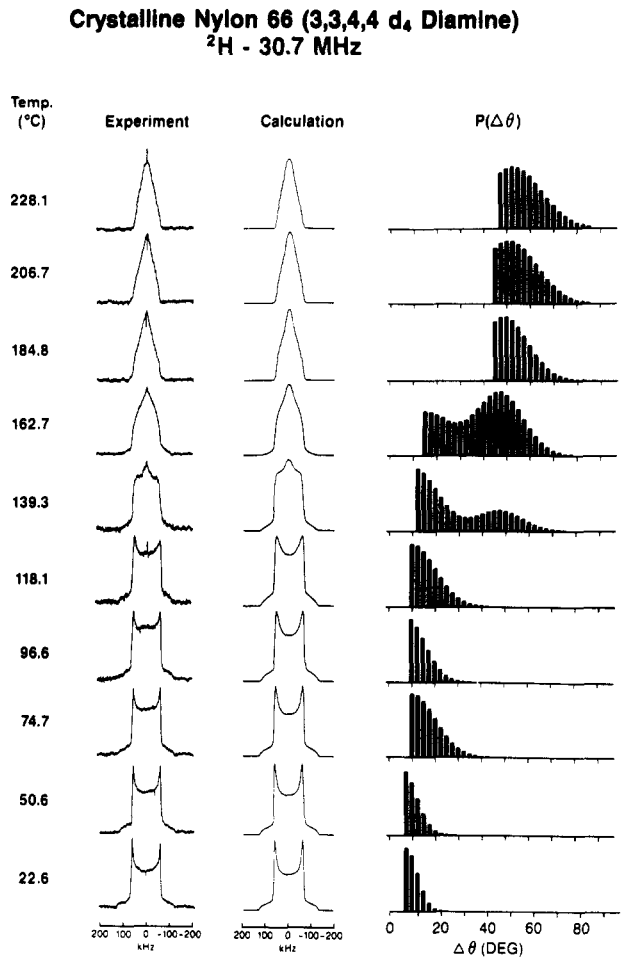

Figure 14. Experimental and calculated ^2H NMR line shapes with the distribution of standard deviations of Gaussian librations used in the calculations for the long-T_1 component (crystalline fraction) of NY34NHME. At the three highest temperatures, a biaxial librational model has been used where the mean value of the second librational distribution at each temperature is 5.4° (184.8 °C), 7.1° (206.7 °C), and 9.8° (228.1 °C).

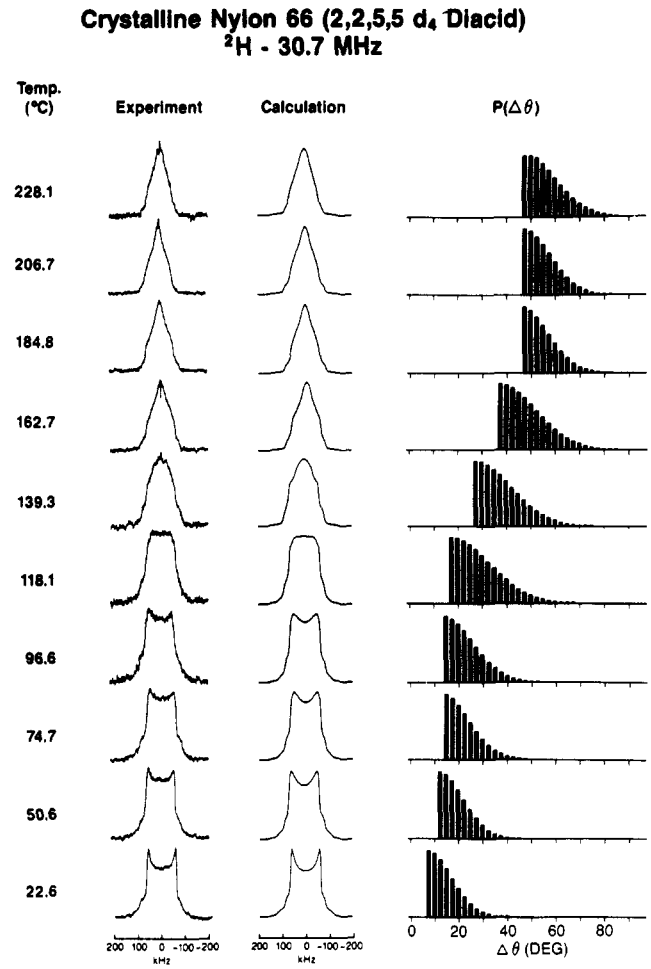

Figure 15. Experimental and calculated ^2H NMR line shapes with the distribution of standard deviations of Gaussian librations used in the calculations for the long-T_1 component (crystalline fraction) of NY25COME.

here.[53,54] Second, the tgtg′ sequences may easily reorient from left to right handed: gtg′ ↔ g′tg.[50] Such a motion would populate a third jump site and would not yield line shapes consistent with the experimental results. This same inconsistency would apply to crank-like counterrotations of second-neighbor bonds like ttt ↔ gtg′ or ttt ↔ g′tg.[14,57,58] Thus, we may conclude that the two-site near tetrahedral jump model (trans–gauche conformational isomerization) is consistent with neither the shortening of the chain axis nor the NMR line shapes.

The model of motion successfully employed for the C–D groups was large-amplitude uniaxial libration about the main chain bonds and is used here to fit not only the data discussed above but also anisotropic relaxation data. Such a motion has already been proposed based upon the results of both NMR and X-ray studies,[48,55,59] but these previous studies lacked the molecular specificity to determine what role the amide groups played in the proposed motion. From the experimental line shapes, it is clear that all of the methylene groups must participate in the motion. We assume that the rotations operate in a concerted counterrotational manner[14,57] about the odd bonds (the first odd bond in each moiety is the bond between the amide moiety and the adjacent methylene group), which stay approximately parallel to each other, with the even bonds staying essentially in the trans configuration. This motion permits small translations of the amide groups but not rotations. The librations are chosen to be Gaussian (see above and Appendix B), and an inhomogeneous distribution of these librations ($P(\Delta\theta)$) is necessary to fit the experimental data. The analytical form of $P(\Delta\theta)$ is not uniquely determined by the data but is chosen to be a half-Gaussian for all of the line shapes of the adipoyl moiety and the HMDA line shapes below the Brill transition. For the HMDA line shapes near and above the Brill transition, a second Gaussian distribution at larger angles was added which also uses a variable low-angle cutoff. It is clear that other analytical expressions could have been used, but the general shape determined for $P(\Delta\theta)$ is believed to be correct, and in particular the bimodal character observed in the HMDA moiety at and above the Brill transitions is not an artifact. This observation of bimodality in the HMDA line shapes only at 139 and 163 °C is in complete accord with the X-ray data (see Appendix C), which finds the presence of two crystallographic phases present in the range 130–170 °C. It is not clear to us why this bimodality is observed only in the HMDA moiety and not in the adipoyl moiety.

Figure 17 illustrates the mean librational angle amplitude $\langle\Delta\theta\rangle$ for each type of methylene group. The mean librational amplitude for each methylene group within each moiety is seen to be very similar at all temperatures in accord with the original qualitative observations. Below the Brill transition (130 °C), the shape of $P(\Delta\theta)$ is half-Gaussian for all methylene groups, and the mean librational amplitudes indicate that the amplitude of motion in the adipoyl moiety is larger than in the HMDA

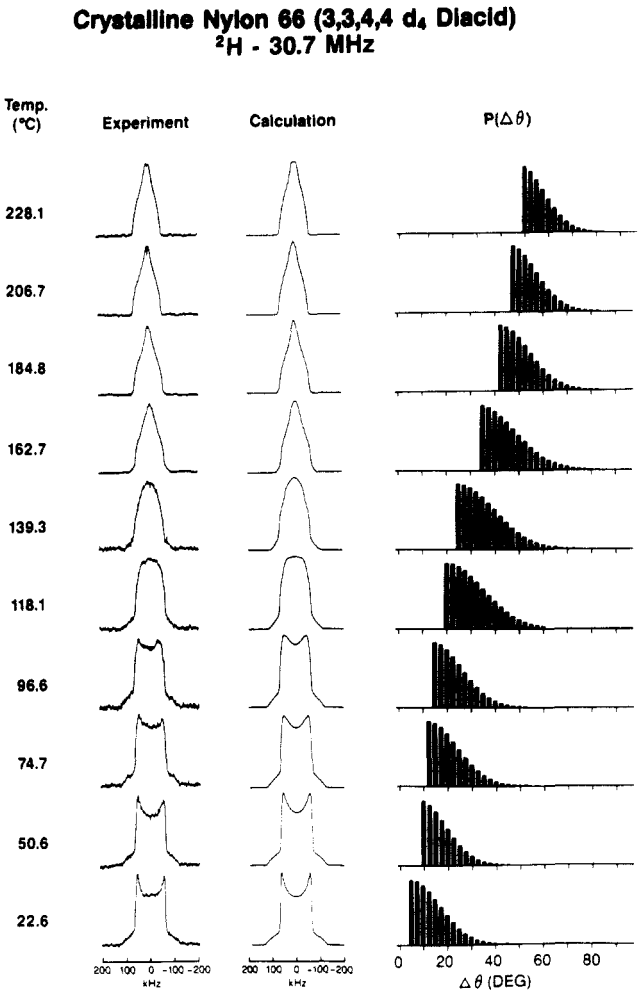

Figure 16. Experimental and calculated ^2H NMR line shapes with the distribution of standard deviations of Gaussian librations used in the calculations for the long-T_1 component (crystalline fraction) of NY34COME.

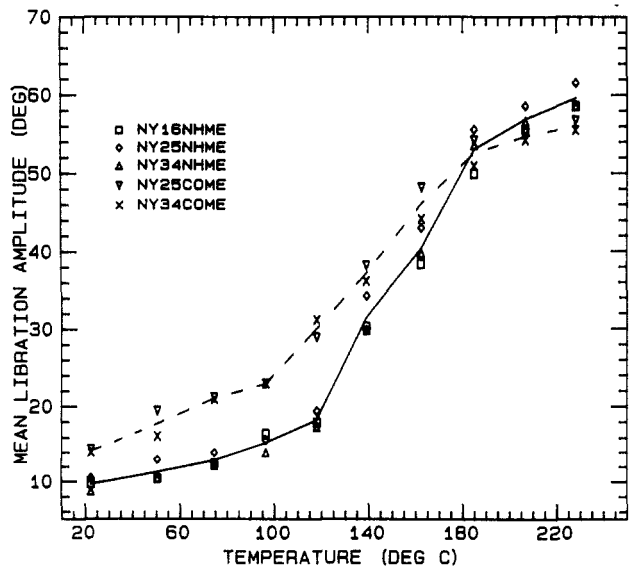

Figure 17. Temperature dependence of the mean librational amplitude of each of the chemically distinct C–D bonds of nylon 66 located within a crystalline domain.

moiety, once again in accord with the original qualitative observations. In the range of the Brill transition (130–170 °C), $P(\Delta\theta)$ is bimodal only for the HMDA segments and not the adipoyl segments, as discussed above. Above the Brill transition (above 170 °C), $P(\Delta\theta)$ is close to being half-Gaussian again, and the mean librational amplitudes are now quite similar for all methylene groups, again in accord with previous qualitative observations. Above this temperature, it was also necessary to add in a small amount of libration in the polar angle β, to account for a reduction in the the overall width of the line shape; values for the mean value $\langle\Delta\beta\rangle$ of this second librational distribution ($P(\Delta\beta)$) are given in Figures 13 and 14. This second librational motion may reflect a nonnegligible amount of libration about each even bond in the interior methylene groups within the HMDA moiety at the three highest temperatures.

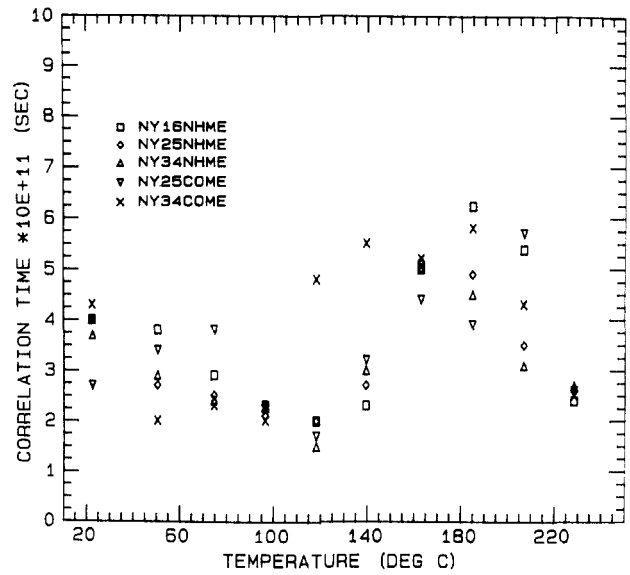

Figure 18. Temperature dependence of the mean correlation time, $2\pi\tau_c$, for the librational motion of each methylene group of nylon 66 located within a crystalline domain.

The librational motion that we have used to model the motion in the methylene chains accounts for not only the NMR line shapes but also the decrease in the stem length with temperature and the increase of the interchain separation between the hydrogen-bonded sheets.[48,55,56] The hydrogen bonds keep the dimension within the hydrogen-bonded sheets constant[48,56] (see above) and do not allow the formation of gauche bonds.

Rate of C–D Librational Motion. Figure 12 illustrates the absence of any significant anisotropy of T_2 relaxation in the line shapes of NY16NHME at temperatures in the region of the Brill transition. These data in conjunction with similar data at both lower and higher temperatures for all six labeled polymers indicate that the motion responsible for the observed line shape changes as a function of temperature must be rapid on the time scale of this experiment, $1/\nu_Q \sim 10^{-5}$ s. In order to quantitatively determine the rate of the librational motion, we have analyzed the spin–lattice relaxation data, which are sensitive to both the rate and amplitude of the motion in conjunction with the knowledge of the amplitude of motion from the line-shape analysis to extract a mean value for the correlation time characterizing this motion. This treatment is detailed in Appendix D, and Figure 18 illustrates the temperature dependence of the librational mean correlation time $2\pi\tau_c$. This mean correlation time for each of the methylene C–D bonds is in the range 20–60 ps over the entire temperature range examined. Given the very minor temperature dependence of the mean correlation time, the decrease in the spin–lattice relaxation time with temperature is mainly a reflection of the growth in amplitude of the motion. As an aside, we note that the same variation of τ_c with temperature is obtained for a model using a two-site trans-

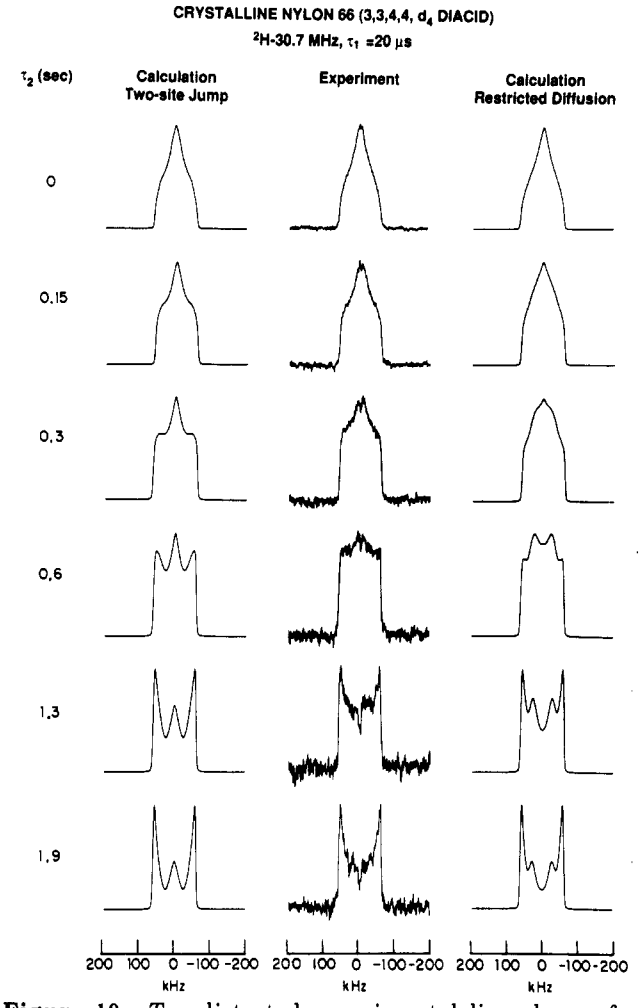

Figure 19. T_{1Q} distorted experimental line shapes for NY34COME at 184.8 °C as a function of τ_2. Calculated line shapes for two models of motion: left-hand side is for a two-site jump (jump angle $2\beta = 90°$) with a half-Gaussian inhomogeneous distribution of site populations P centered at $P_0 = 0.66$ and of standard deviation $\Delta P = 0.08$, truncated at $P = 0.5$; right-hand side is for a restricted diffusion model with a half-Gaussian inhomogeneous distribution of diffusion amplitudes ψ_l centered at $\psi_{l0} = 68°$ and of standard deviation $\Delta\psi_l = 9°$. For both simulations, $\nu_c = (2\pi\tau_c)^{-1} = 10^{10}$ Hz.

gauche jump where the relative site populations approach 1/1 as the temperature is increased. Therefore, the decrease of T_1 with increasing temperature does not reflect an increasing rate of random motions in a thermally activated process but rather an increasing amplitude of the random fluctuation. This clearly indicates that a trans–gauche conformational isomerization model is inappropriate and that the librational model is correct.

Further information on both the time scale and geometry of motion is available from consideration of the orientational dependence of the spin–lattice relaxation. In particular, it has been shown[34] that the strong anisotropy of spin alignment spin–lattice relaxation (T_{1Q}) can readily distinguish between large-angle uniaxial (ψ_l) restricted diffusion and trans–gauche two-site jumps. Figure 19 shows the distortions obtained at 184.8 °C for NY34COME. The τ_2 dependence of the echo amplitude is well fit by a biexponential decay with time constants of 40 and 630 ms (amplitude 46%). The latter of these is associated with crystalline domains, and the ratio of this value of T_{1Q} to T_1 at this same temperature is 1.55, which is quite close to the theoretical value of 1.67 ($\omega\tau_c \ll 1$)[23] and confirms that the τ_2 decay is entirely due to the spin–lattice relaxation and that there is no additional echo intensity reduction due to slow molecular reorientation.[23] (Note that for the present case T_{1Q}-distorted line shapes of the crystalline domains can be directly obtained without any signal manipulation since the noncrystalline component decays much more rapidly than the crystalline component.) The undistorted spectrum ($\tau_2 = 0$) obtained by the solid echo sequence is very close to an $\eta^* = 1$, $\nu_Q^* = \nu_Q/2$ line shape. If the motion is a two-site jump, strong central singularities are observed when $\tau_2 \gg 0$.[34] Experimentally, no central singularities are observed. Since the splitting of these central peaks is independent of τ_c,[34] they cannot be smeared out by any distribution of correlation times.

Alternatively, they can be smeared out by an inhomogeneous distribution of trajectories of motion (amplitudes). This type of distribution is what is concluded from the line-shape analysis. Note that for the unique case of equally populated sites the splitting of the central peaks is the same for any jump angle so that a distribution of jump angles would not smear out the central peaks. In an attempt to fit the T_{1Q} data with a two-site jump model, a distribution of populations is more effective at smearing the central peaks, and this calculation is shown on the left-hand side of Figure 19; however, even for this model a relatively large central peak is still present at long values of τ_2. This result indicates that no two-site jump model can fit the experimental data. On the other hand, restricted uniaxial diffusion has been shown[34] to yield very weak central peaks. Unfortunately, the frequencies of these very weak singularities are independent of the width of the diffusion profile; however, the right-hand side of Figure 19 illustrates that this model gives a much better fit to the experimental data than the two-site jump model. This model uses a rectangular well potential, and the use of a more physically realistic potential might give even better agreement than that already found. Thus, all of the spin–lattice relaxation data (T_1 and T_{1Q}) show that the motion responsible for the averaging observed in the line shapes does not arise from discreet trans–gauche conformational isomerization but rather from very rapid large-amplitude librations which can be modeled as uniaxial restricted diffusion. Lastly, note that the correlation time ($2\pi\tau_c = 100$ ps) used to fit the T_{1Q}-distorted line shapes is quite close to the value determined from the T_1 data (60 ps).

Influence of Water on C–D Librational Motion. Figure 20 illustrates that the temperature-dependent line shapes of the crystalline portions of NY25NHME and NY34COME are essentially unaffected by the presence of 2 ± 0.3 wt % water. Similar results are found for the other C–D bonds in the repeat unit. Figure 21 illustrates that the type of motion extant in the wet nylon not only gives very similar line shapes to that observed for the dry nylon but that the motion does not give rise to any T_2 anisotropy and hence must be quite rapid on this time scale. These observations that the introduction of water has no effect on the dynamics in the crystalline phase are in agreement with the general belief that either water does not penetrate the crystal or the equilibrium concentration is quite small.[60,61]

Nylon 66 Crystal Structures from Room Temperature to 228 °C. X-ray diffraction data for nylon 66 melt-recrystallized polymer as a function of temperature are described in Appendix C. Detailed analysis of these data indicates that below 130 °C the scattering pattern is consistent with the presence of only one crystalline phase (triclinic) and above 180 °C is again consis-

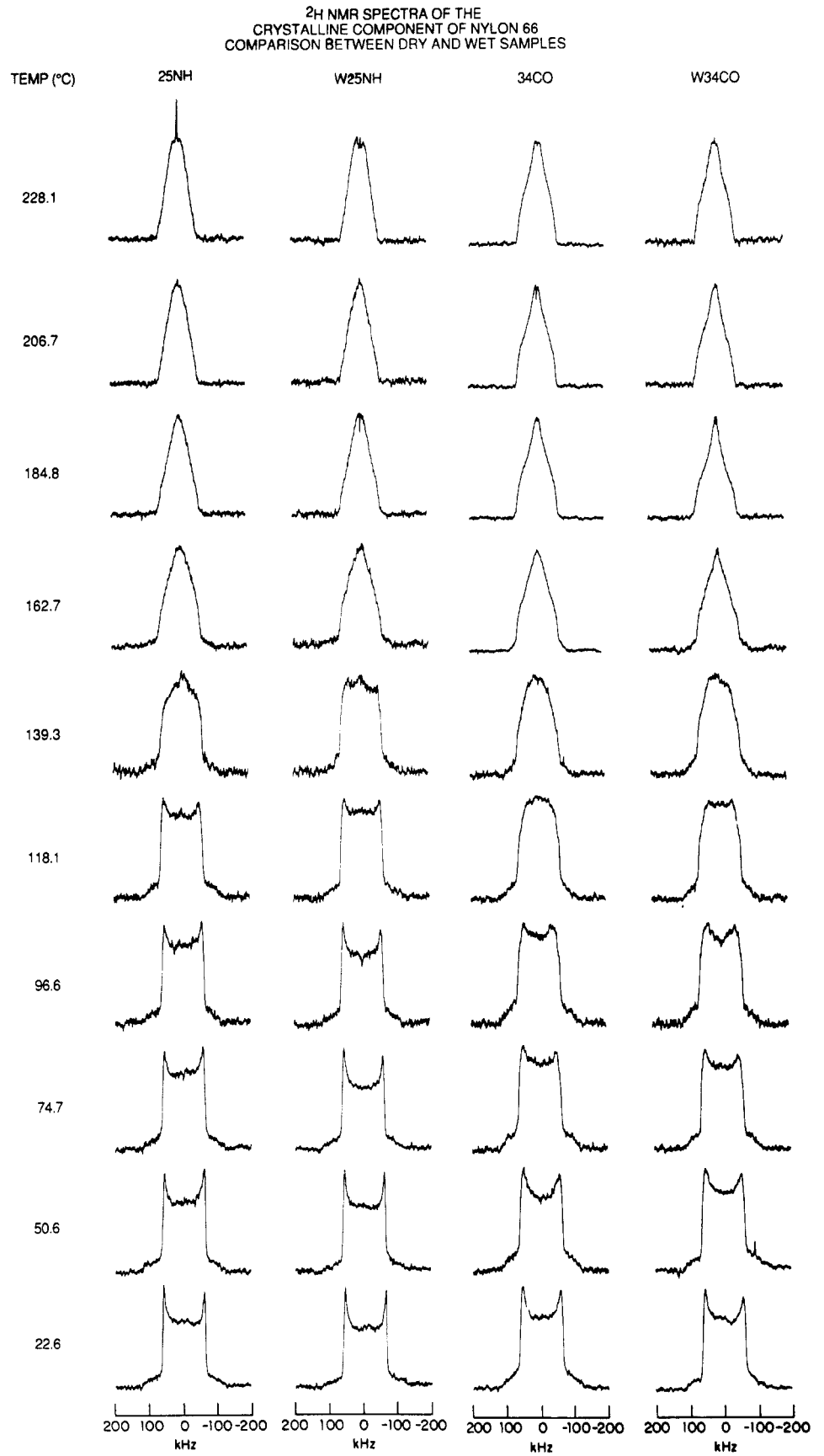

Figure 20. Experimental ^2H NMR line shapes, as a function of temperature, for the crystalline portion of NY25NHME (dry) (left column), WNY25NHME (NY25NHME + 2 ± 0.3 wt % water) (one column from the left), NY34COME (dry) (one column from the right), and WNY25NHME (NY25NHME + 2 ± 0.3 wt % water) (far right column).

tent with the presence of only one crystalline phase (triclinic or pseudohexagonal). In the intermediate temperature range, the data can only be fit with the simultaneous presence of both of these crystallographic phases. This finding is consistent with the small lamellar thickness[16] of this polymer giving rise to substantial structural heterogeneity allowing surface effects to play a substantial role in the energetics of the Brill transition. Note

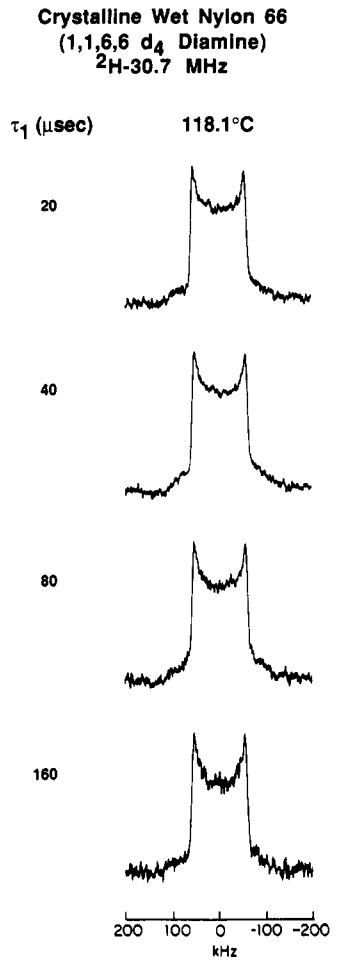

Figure 21. Experimental ^2H NMR line shapes for the crystalline fraction of WNY16NHME (NY16NHME + 2 ± 0.3 wt % water) as a function of the delay time (τ_1) at 118.1 °C.

that the simultaneous presence of two crystalline forms in this temperature range is directly reflected in the C–D dynamics in the HMDA moiety near the Brill transition; furthermore, the gross structural heterogeneity may be the origin of the large amount of inhomogeneity observed in the librational motion of all C–D bonds above room temperature. Lastly, recently reported DSC results have shown that the excess heat capacity associated with the Brill transition is quite diffuse and extends over the temperature range 140–220 °C.[66]

Summary

First, the magnetization in selectively deuterated nylon 66 polymers may be effectively partitioned, via spin–lattice relaxation discrimination, between that arising from crystalline domains and that from noncrystalline domains. This discrimination appears to be quite effective above −50 °C because there exists sufficiently different motion in the two domains that the T_1 values differ by minimally a factor of 24 over the range −50 to 228 °C. The value of the fraction of magnetization corresponding to the long-T_1 component is in the range 32–47% over this temperature range, and this compares well with the values of 39% (DSC) and 35% (X-ray diffraction at 25 °C). Furthermore, the long-T_1 component is associated with the line shape which shows much less motional averaging than do the line shapes associated with the short-T_1 component.

Second, the amide N–D groups show evidence of very little rotational motion up to 228 °C, which is quite near the melting temperature of 250–260 °C. The minor amount of motion present is well described as a restricted, rapid, spatially inhomogeneous libration. The mean correlation time for this motion is found to vary from 500 to 200 ps over the range 185–228 °C. This type of motion indicates that previously proposed models[49,62] which claimed that the chains jump 60° about their long axes, thus giving rise to a three-dimensional hydrogen-bonded network in the pseudohexagonal structure, are incorrect.

Third, the methylene C–D bonds show evidence of much more motion than is present in the N–D bonds. The motion of the C–D groups is a large-amplitude, rapid, spatially inhomogeneous libration based upon the results of the line-shape simulations, the lack of anisotropy of the T_2 relaxation, and the T_{1Q} results. (No type of a two-site jump such as a trans–gauche isomerization is consistent with all of the experimental data.) The mean correlation time of this motion is found to be in the range 20–60 ps over the entire temperature range examined (25–228 °C) and is much too rapid to be detected in any mechanical or dielectric relaxation experiment. Indeed, the observation that the amplitude of the T_1 components is essentially independent of temperature requires that there never be a significant fraction of the magnetization in the intermediate-exchange regime; therefore, the motion in the crystalline domains must be rapid at all temperatures with a growth in amplitude to account for this observation. The virtually identical amount of motional averaging that occurs within each moiety at all temperatures is suggestive of a concerted counterrotation about odd bonds within each methylene chain with the libration about the 1,5 (adipoyl moiety) and 1,7 (HMDA moiety) bonds being the prevalent modes of motion. (The presence of virtually identical motion for each methylene group within each moiety for the crystalline domains may be compared to that observed in the noncrystalline domains, where the terminal methylene groups within each moiety are hindered relative to the interior methylene groups.) This type of cooperative motion would be consistent not only with the NMR data but also the X-ray data as to the contraction of the c-axis with increasing temperature (Appendix C and ref 63). Furthermore, this model is consistent with the low entropy of fusion present in nylon 66.[64]

Below the Brill transition, the observation of larger amplitude motion within the shorter methylene segment (adipoyl moiety) appears to be somewhat anomalous. This result may be rationalized by examination of the chain geometry which shows evidence of larger steric hindrance between the terminal C–H bonds of the HMDA moiety and the adjacent C=O groups as compared to the steric hindrance of the C–H bonds of the terminal methylene groups in the adipoyl moiety and the adjacent N–H groups. This rationalization of the presence of larger amplitude motion in the adipoyl moiety below the Brill transition, as well as the type of motion that the C–H undergo, is in excellent agreement with the results of molecular dynamics computer simulations.[65]

Fourth, the C–D dynamics in the HMDA moiety in the range of the Brill transition are sensitive to the simultaneous presence of two crystallographic phases for this diffuse structural transition.

Fifth, the introduction of 2 ± 0.3 wt % of water into the polymer has no effect on the observed line shapes or relaxation behavior of the crystalline domains of nylon 66. This result is quite different than that found for the amorphous domains (see following paper).

Acknowledgment. We are indebted to H. A. Holyst

and P. A. Cooper for skilled technical assistance and to G. A. Jones for acquisition of the X-ray diffraction data. It is also a great pleasure to acknowledge Dr. Rudolph J. Angelo for his preparation of all of the polymers used in this work and many useful discussions.

Appendix A. Matrix Method of Least-Squares Fitting

For the evaluation of the time domain spin–lattice relaxation data, the data are fit to two or more time constants and one or more parameters which describe how the magnetization is partitioned in a two or more phase model. Least-squares fitting of the data to such a model may be accomplished by a brute force fitting of the three or more independent parameters to eq A1

$$M(t) = M_0[(a_1)(1 - e^{-t/T(a_1)}) + (a_2)(1 - e^{-t/T(a_2)}) + \ldots (a_k)(1 - e^{-t/T(a_k)})] \quad \text{(A1)}$$

where M_0 is the equilibrium magnetization, t is time, $M(t)$ is the value of the magnetization as a function of the recovery time after the presaturation sequence, $T(a_1)$, $T(a_2)$, and $T(a_k)$ are the spin–lattice relaxation times of the two or more phases, and the sum of all a_k is unity.

However, this approach is rather inefficient, and a much simpler and more effective method is a Newton–Raphson iteration in matrix form.[67,68] For clarity, we write $M(t)$ as an explicit function of not only time but also all other parameters $(x_1, x_2, x_3, x_4, \ldots, t)$ upon which it depends. The experimentally determined value will be $M_e(t)$, and the calculated value will be $M_c(t)$. The difference between the experimental and calculated values is just

$$\Delta M(t) = M_e(t) - M_c(t) \quad \text{(A2)}$$

where t takes values from t_1 to t_m.

If the differences between the actual values of x_i ($x_i(a)$) and the calculated values of x_i ($x_i(c)$) are sufficiently small, then the following relationship is valid:

$$\Delta M(t) = (\partial M(t)/\partial x_1)\Delta x_1 + (\partial M(t)/\partial x_2)\Delta x_2 + \ldots (\partial M(t)/\partial x_n)\Delta x_n \quad \text{(A3)}$$

where

$$\Delta x_n = x_n(a) - x_n(c) \quad \text{(A4)}$$

A simultaneous set of equations of the form of eq A3 may be written in matrix form as

$$\Delta \mathbf{M}^* = \Phi^* \cdot \Delta \mathbf{x}^* \quad \text{(A5)}$$

where

$$\Delta \mathbf{M}^* = \begin{bmatrix} \Delta M(t_1) \\ \Delta M(t_2) \\ \cdots \\ \cdots \\ \Delta M(t_m) \end{bmatrix}$$

$$\Delta \mathbf{x}^* = \begin{bmatrix} \Delta x_1 \\ \Delta x_2 \\ \cdots \\ \cdots \\ \Delta x_n \end{bmatrix}$$

$$\Phi^* = \begin{bmatrix} \partial M(t_1)/\partial x_1 & \partial M(t_1)/\partial x_2 & \cdots & \partial M(t_1)/\partial x_n \\ \partial M(t_2)/\partial x_1 & \partial M(t_2)/\partial x_2 & \cdots & \partial M(t_2)/\partial x_n \\ \cdots & \cdots & \cdots & \cdots \\ \cdots & \cdots & \cdots & \cdots \\ \cdots & \cdots & \cdots & \cdots \\ \partial M(t_m)/\partial x_1 & \partial M(t_m)/\partial x_2 & \cdots & \partial M(t_m)/\partial x_n \end{bmatrix}$$

We may calculate values of ΔM^* from an initial guess or the most recently calculated value and the experimental data using eq A2. Φ^* may be numerically calculated from eq A1. Thus we may calculate Δx^* from eq A5 and obtain all values of $x_n(a)$ from eq A4; the new values of $x_n(a)$ become the values of $x_n(c)$ in the next iteration.

This procedure is trivial so long as Φ^* has an inverse. This is not the usual case, because Φ^* is not square. This problem can be circumvented by multiplying both sides of eq A5 by Φ^{*T} to give

$$\Phi^{*T} \cdot \Delta \mathbf{M}^* = \Phi^{*T} \cdot \Phi^* \cdot M\mathbf{x}^* \quad \text{(A6)}$$

If the matrix $\Phi^{*T} \cdot \Phi^*$ is nonsingular, it can be numerically inverted and thus

$$\Delta \mathbf{x}^* = [\Phi^{*T} \cdot \Phi^*]^{-1} \Phi^{*T} \Delta \mathbf{M}^* \quad \text{(A7)}$$

In practice, to avoid numerical instability, we only increment the new values of $x_n(c)$ by 0.75 Δx_n. After several iterations of this calculation, convergence is rapidly achieved if the form of eq A1 properly describes the data and the experimental data are at least of reasonable quality.

Appendix B. Gaussian Distribution of Librational Angles in the Harmonic Oscillator Approximation

A Gaussian distribution of populations has been used in the model for librational motion in the line-shape calculations. This distribution can be shown to be an extremely good approximation for a harmonic oscillator. The eigenfunctions, ψ_v, of a harmonic oscillator are given by[69]

$$\psi_v(y) = N_v e^{(-y^2/2)} H_v(y)$$

where N_v is the normalization factor to yield an orthonormal set, y is the displacement variable, and $H_v(y)$ are the Hermite polynomials. It is clear that the coefficients of the Hermite polynomials are Gaussian, but the probability distributions in each eigenstate are not Gaussian. The ensemble average probability distribution as a function of temperature may be calculated by summing the probability distribution of each state $\langle \psi_v(y)^* \psi_v(y) \rangle$ over an ensemble of states.

Such a calculation for ethane, when approximated as a harmonic oscillator, with $\nu_0 = 300$ cm^{-1} and only the eigenstates from $v = 0$ to 10 considered, gives a population distribution which is very well approximated by a Gaussian from 0 to 1400 K; above this temperature the distribution departs from Gaussian because levels above $v = 10$ must be accounted for at these temperatures. Clearly, at very high temperatures, the internal rotation potential for ethane cannot be approximated as a harmonic oscillator. However, at the temperatures employed in this work (<500 K, which corresponds to approximately 1/3 of the barrier height used in this example) this approximation for ethane is acceptable. So long as the barrier to methylene group internal rotation in nylon 66 is larger or comparable to the internal rotation barrier in ethane, the ensemble average probability distribution should be well approximated as Gaussian. Note that at all temperatures this distribution must have a standard deviation greater than zero; therefore, even at a temperature of absolute zero the distribution has finite width.

Appendix C. Temperature Dependence of the Unit Cell of Nylon 66

Figures 22, 23, and 24 respectively show the diffraction patterns (5–30° 2Θ) of melt-recrystallized nylon 66

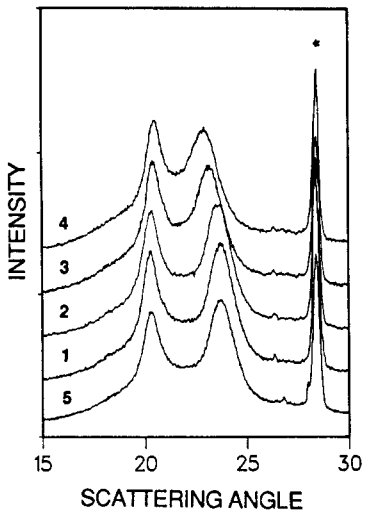

Figure 22. X-ray diffraction pattern of melt-recrystallized nylon 66 polymer as a function of temperature below the Brill transition: 1, 25 °C; 2, 62 °C; 3, 100 °C; 4, 120 °C; 5, 25 °C after the polymer had been heated to 240 °C. The peak marked with an asterisk is due to the silicon internal standard.

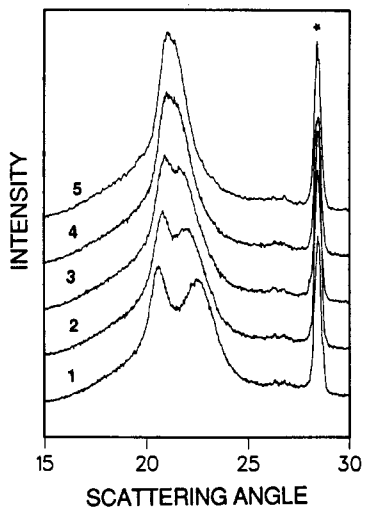

Figure 23. X-ray diffraction pattern of melt-recrystallized nylon 66 polymer as a function of temperature near the Brill transition: 1, 140 °C; 2, 160 °C; 3, 170 °C; 4, 180 °C; 5, 190 °C.

in the temperature ranges 25–120, 140–190, and 200–240 °C. Included in Figure 22 is the diffraction pattern obtained at 25 °C after the sample had been cooled from 240 °C. The pattern is identical with that of the original sample, thus confirming that there have been no irreversible changes in the sample when the ceiling temperature does not exceed 240 °C.

The diffraction patterns recorded at or below 120 °C (Figure 22) can be indexed by a simple one-chain triclinic unit cell. The unit-cell parameters calculated from the 25 °C diffraction pattern are a = 0.496 (2) nm, b = 0.552 (1) nm, c = 1.741 (2) nm, α = 48.0° (2)°, β = 76.1° (2)°, and γ = 62.1° (2)° and indicate that the polymer is in the α crystal form. This unit cell is in good agreement with the room temperature unit-cell parameters previously reported.[46,48,56,63]

The diffraction patterns recorded at or above 190 °C, above the Brill transition, can be indexed by a one-chain triclinic (pseudohexagonal) unit cell with dimensions a = 0.491 (1) nm, b = 0.587 (1) nm, c = 1.650 (2) nm, α = 55.7° (10)°, β = 80.7° (3)°, and γ = 60.1° (2)°. Again, the derived unit-cell parameters are consistent with those reported in the literature.[48,63] Starkweather and Jones[56] have reported a c-axis parameter of 1.718 nm for solution-crystallized polymer, which is significantly longer than that found here and elsewhere[48,63] for melt-crystallized polymer.

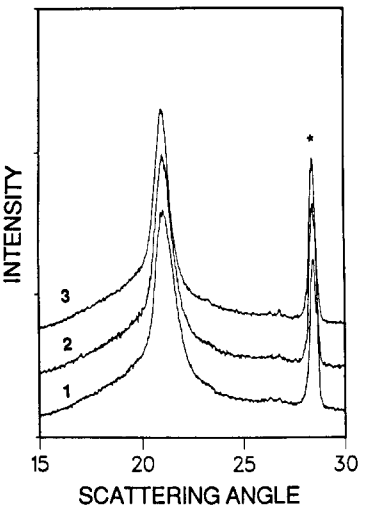

Figure 24. X-ray diffraction pattern of melt-recrystallized nylon 66 polymer as a function of temperature above the Brill transition: 1, 200 °C; 2, 210 °C; 3, 220 °C.

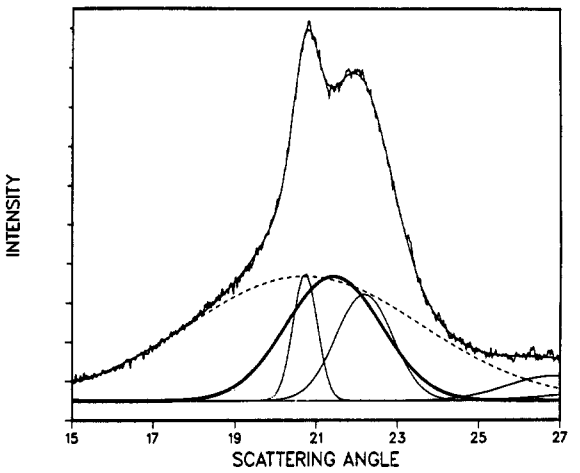

Figure 25. X-ray diffraction pattern of melt-recrystallized nylon 66 polymer at 160 °C and component Gaussian peaks obtained by deconvolution. Scattering features associated with the amorphous phase (dashed line) and the crystalline phase found both above (bold line) and below (solid line) the Brill transition are shown.

In the intermediate temperature range, the diffraction patterns could not be successfully treated assuming that there was a single unit cell. Rather, it was necessary to assume that the low- and high-temperature forms of the polymer must coexist to account for the observed scattering. Figure 25 shows the diffraction pattern collected at 160 °C deconvoluted into Gaussian peaks. In addition to the broad scattering component from the noncrystalline polymer, scattering features associated with the crystalline phase found above (bold line) and below (solid line) the Brill transition are observed. These observations confirm the NMR results that the Brill transition is very broad and that the transition temperature is probably dependent on the size and perfection of the crystals.

Appendix D. Calculation of the Powder Average Spin-Lattice Relaxation Time

We first define (θ_p, ϕ_p) and (β, ψ) as the spherical coordinates specifying the respective orientations of the external static magnetic field H_0 and the unique principal axis

of the field gradient tensor ($\eta = 0$) in an arbitrary molecular axis system. The general expression of the spin–lattice relaxation time T_1 due to the quadrupolar coupling of a ^2H nucleus of quadrupolar coupling constant ν_Q is written[39]

$$1/T_1 = (3/4)(\pi\nu_Q)^2[J_1(\omega) + 4J_2(2\omega)] \quad \text{(D1)}$$

The spectral density functions are defined as

$$J_m(\omega) = 2\int_0^\infty C_m(t) \cos(\omega t)\, dt \quad \text{(D2)}$$

The autocorrelation function is given by

$$C_m(t) = \sum_{a,a'=-2}^{2} d^2_{ma}(\theta_p) d^2_{ma'}(\theta_p) \exp[i(a - a')\phi_p] C_{aa'}(t) \quad \text{(D3)}$$

where the d^2_{ma} are the usual reduced second-rank Wigner rotation matrix elements.[35] The $C_{aa'}(t)$ are the correlation functions describing the reorientation of the unique principal axis in the arbitrary molecular axis system (i.e., they only depend on β and ψ).

For an anisotropic motion in a solid, T_1 generally depends on the orientation (θ_p, ϕ_p); hence the relaxation is nonexponential.[39] This property can be used to differentiate motions giving rise to equivalent fast-exchange line shapes.[28,39] However, nonexponential T_1 effects are generally weak,[34,39] and given the relatively low precision of the experimental T_1 values we shall assume that the crystalline relaxation is well described by the powder average spin–lattice relaxation time T_1^*. T_1^* is then given by replacing $J_m(\omega)$ by $J_m^*(\omega)$ in eq D1, the star denoting the powder average. Similarly, $J_m^*(\omega)$ is the Fourier transform of $C_m^*(t)$ (eq D2). We then have

$$C_m^*(t) = (1/4\pi)\int_0^{2\pi}\int_0^{\pi} C_m(t) \sin\theta_p\, d\theta_p\, d\phi_p \quad \text{(D4)}$$

It is readily seen that only the terms with $a = a'$ are non-zero:

$$\int_0^{2\pi} \exp[i(a - a')\phi_p]\, d\phi_p = 0 \quad \text{if } a \neq a'$$
$$= 2\pi \quad \text{if } a = a' \quad \text{(D5)}$$

It is also easily verified that for $m = 1, 2$ and $a = -2, \ldots 2, 2$

$$\int_0^{\pi} [d^2_{ma}(\theta_p)]^2 \sin\theta_p\, d\theta_p = 2/5 \quad \text{(D6)}$$

From eqs D4–D6 we then obtain

$$C_1^*(t) = C_2^*(t) = (1/5)\sum_{a=-2}^{2} C_{aa}(t) \quad \text{(D7)}$$

Furthermore, if the motion is uniaxial (β is constant)[39]

$$C_{aa}(t) = [d^2_{0a}(\beta)]^2 \Gamma_{aa}(t) \quad \text{(D8)}$$

where

$$\Gamma_{aa}(t) = \langle \exp(ia[\psi(0) - \psi(t)]) \rangle$$

The brackets ($\langle\ \rangle$) denote the ensemble average over the motion. Since we are interested in the spin–lattice relaxation, only the time-dependent part of $\Gamma_{aa}(t)$, called $\Gamma'_{aa}(t)$, is relevant. $\Gamma'_{aa}(t)$ can be expressed as[35]

$$\Gamma'_{aa}(t) = [\Gamma_{aa}(0) - \Gamma_{aa}(\infty)]g(t) = \Delta\Gamma_{aa} g(t) \quad \text{(D9)}$$

where $g(t)$ is the normalized correlation function ($g(0) = 1$). $g(t)$ contains all the information about the time scale of the motion, and $\Delta\Gamma_{aa}$ depends solely on the spatial averaging of the interaction. Indeed, $\Gamma_{aa}(0) = \langle|\exp[ia\psi]|^2\rangle = 1$ and $\Gamma_{aa}(\infty) = |\langle\exp[ia\psi]\rangle|^2 = \langle\cos a\psi\rangle^2 + \langle\sin a\psi\rangle^2$ are easily calculated according to the time-averaged azimuthal distribution $P(\psi)$. In the case of a simple two-site jump motion, $g(t) = \exp(-t/\tau_c)$ with $(\tau_c)^{-1}$ the sum of the rate constants ($k_{12} + k_{21}$) for jumping from one site to the other.[39] For a two-site jump of angle 2β with site populations P_1 and P_2, it is then readily found that

$$C_m^*(t) = (3/5)P_1P_2 \sin^2(2\beta) \exp(-t/\tau_c) \quad \text{(D10)}$$

For other more complicated motions, $g(t)$ is generally not exponential.[39] For a model of restricted diffusion between $\pm\psi_l$, $g(t)$ is found to be a rapidly converging series of exponential terms which may be approximated by the leading term.[34] For a Gaussian libration of standard deviation $\Delta\theta$ symmetric about $\psi = 0$ ($P(\psi) = P(-\psi)$), we have $\langle\sin a\psi\rangle = 0$ and $\langle\cos a\psi\rangle = \exp[-(a\Delta\theta)^2/2]$, and $C_m^*(t)$ is given by

$$C_m^*(t) = (3/20)(\sin^4\beta[1 - \exp(-4\Delta\theta^2)] + 4\cos^2\beta \sin^2\beta[1 - \exp(-\Delta\theta^2)])g(t) \quad \text{(D11)}$$

The shape of $g(t)$ will depend on the details of the librational motion; in order to get an estimation of the correlation time, $g(t)$ is conveniently approximated by $\exp(-t/\tau_c)$.

The spatial averaging reflected by $\Delta\Gamma_{aa}$ is directly given by the analysis of the line shapes. Therefore, the spin–lattice relaxation time T_1^*, corresponding to the distributions of libration amplitudes $P(\Delta\theta)$ deduced from the line-shape analysis, may be computed. Comparison with the experimental T_1 values permits determination of the temperature dependence of a mean correlation time τ_c for each labeled methylene group (Figure 18).

References and Notes

(1) Spiess, H. W. *Colloid Polym. Sci.* **1983**, *261*, 193.
(2) Cohen-Addad, J. P. *Polymer* **1983**, *24*, 1128.
(3) English, A. D. *Macromolecules* **1985**, *18*, 178.
(4) Jones, A. A. *Molecular Dynamics in Restricted Geometries*; Klaster, J.; Drake, J. M., Eds.; Wiley: New York, in press.
(5) Wehrle, M.; Hellmann, G. P.; Spiess, H. W. *Colloid Polym. Sci.* **1987**, *265*, 815.
(6) Vega, A. J.; English, A. D. *Macromolecules* **1980**, *13*, 1635.
(7) Hentschel, D.; Sillescu, H.; Spiess, H. W. *Polymer* **1984**, *25*, 1078.
(8) English, A. D. *Macromolecules* **1984**, *17*, 2182.
(9) English, A. D. *J. Polym. Sci., Polym. Phys. Ed.* **1986**, *24*, 805.
(10) English, A. D., presented in part at the 26th ENC Conference, 1985.
(11) English, A. D.; Smith, P.; Axelson, D. E. *Polymer* **1985**, *26*, 1523.
(12) Bates, F. S.; Wignall, G. D.; Koehler, W. C. *Phys. Rev. Lett.* **1985**, *55* (22), 2425.
(13) Stockmayer, W. H. *Pure Appl. Chem. Suppl. Macromol. Chem.* **1973**, *8*, 379.
(14) Helfand, E. *Science* **1984**, *226*, 647.
(15) Ketels, H.; van de Ven, L.; Aerdts, A.; van der Velden, G. *Polym. Commun.* **1989**, *30*, 80.
(16) Angelo, R. J.; Miura, H.; Gardner, K. H.; Chase, D. B.; English, A. D. *Macromolecules* **1989**, *22*, 117.
(17) Bunn, C. W.; Garner, E. V. *Proc. R. Soc. London A* **1947**, *189*, 39.
(18) Bloom, M.; Davis, J. H.; Valic, M. I. *Can. J. Phys.* **1980**, *58*, 1510.
(19) Gerstein, B. C. *Philos. Trans. R. Soc. London A* **1981**, *299*, 521.
(20) Hentschel, R.; Spiess, H. W. *J. Magn. Reson.* **1979**, *35*, 157.
(21) Henrichs, P. M.; Hewitt, J. M.; Linder, M. *J. Magn. Reson.* **1984**, *60*, 280.
(22) Ronemus, A. D.; Vold, R. L.; Vold, R. R. *J. Magn. Reson.* **1986**, *70*, 416.
(23) Spiess, H. W. *J. Chem. Phys.* **1980**, *72*, 6755.
(24) Powles and Strange *Proc. Phys. Soc.* **1963**, *82*, 6.
(25) Spiess, H. W.; Sillescu, H. *J. Magn. Reson.* **1981**, *42*, 381.
(26) Vega, A. J. *J. Magn. Reson.* **1985**, *65*, 252.

(27) Vega, A. J.; Luz, Z. J. Chem. Phys. 1987, 86, 1803.
(28) Wittebort, R. J.; Olejniczak, E. T.; Griffin, R. G. J. Chem. Phys. 1987, 86, 5411.
(29) Vega, A. J. Polym. Prepr. (Am. Chem. Soc., Div. Polym. Chem.) 1981, 22, 282.
(30) Spiess, H. W. Adv. Polym. Sci. 1985, 66, 23.
(31) Kaplan, J. I.; Garroway, A. N. J. Magn. Reson. 1982, 49, 464.
(32) Mc Call, D. W.; Anderson, E. W. J. Polym. Sci., Polym. Chem. Ed. 1963, 1, 1175.
(33) Miura, H.; English, A. D. Macromolecules 1988, 21, 1543.
(34) Hirschinger, J.; English, A. D. J. Magn. Reson. 1989, 85, 542.
(35) Mehring, M. Principle of High resolution NMR in Solids, 2nd ed.; Springer: New York, 1983.
(36) London, R. E.; Avitabile, J. J. Am. Chem. Soc. 1978, 100, 7159.
(37) Wemmer, D. E. Ph.D. Thesis. Some Double Resonance and Multiple Quantum NMR Studies in Solids. University of California, 1978.
(38) Wemmer, D. E.; Ruben, D. J.; Pines, A. J. Chem. Soc. 1981, 103, 28.
(39) Torchia, D. A.; Szabo, A. J. Magn. Reson. 1982, 49, 107.
(40) Woessner, D. E.; Snowden, B. S., Jr.; Meyer, G. H. J. Chem. Phys. 1969, 51, 2968.
(41) Barbara, T. M.; Greenfield, M. S.; Vold, R. L.; Vold, R. R. J. Magn. Reson. 1986, 69, 311.
(42) Hentschel, D.; Sillescu, H.; Spiess, H. W. Makromol. Chem. 1979, 180, 241.
(43) Pschorn, O.; Spiess, H. W. J. Magn. Reson. 1980, 39, 217.
(44) Jelinski, L. W.; Dumais, J. J.; Engel, A. K. Macromolecules 1983, 16, 492.
(45) Luz, Z.; Vega, A. J. J. Phys. Chem. 1986, 90, 4903.
(46) Bunn, C. W.; Garner, E. W. Proc. R. Soc. 1947, A189, 39.
(47) Chapman, G. E.; Campbell, I. D.; McLaughlan, K. A. Nature 1970, 225, 639.
(48) Colclough, M. L.; Baker, R. J. Mat. Sci. 1978, 13, 2531.
(49) Brill, R. J. Prakt. Chem. 1942, 161, 49.
(50) Boyd, R. H.; Breitling, S. M. Macromolecules 1974, 6, 855.
(51) Huang, T. H.; Skarjune, R. P.; Wittebort, R. J.; Griffin, R. G.; Oldfield, E. J. J. Am. Chem. Soc. 1980, 102, 7377.
(52) Pechhold, W.; Blasenbrey, S.; Woerner, S. Kolloid Z. Z. Polym. 1963, 189, 14.
(53) Boyd, R. H. J. Polym. Sci., Polym. Phys. Ed. 1975, 13, 2345.
(54) Mansfield, M.; Boyd, R. H. J. Polym. Sci., Polym. Phys. Ed. 1978, 16, 1227.
(55) Slichter, W. P. J. Polym. Sci. 1958, 35, 77.
(56) Starkweather, H. W., Jr.; Jones, G. A. J. Polym. Sci., Polym. Phys. Ed. 1981, 19, 467.
(57) Helfand, E. J. Chem. Phys. 1971, 54, 4651.
(58) Skolnick, J.; Helfand, E. J. Chem. Phys. 1980, 72, 5489.
(59) Olf, H. G.; Peterlin, A. J. Polym. Sci., Polym. Phys. Ed. 1971, 9, 1449.
(60) Starkweather, H. W. Water in Nylon. ACS Symp. Ser. 1980, 127, 433.
(61) Murthy, N. S.; Stamm, M.; Sibilia, J. P.; Krimm, S. Macromolecules 1989, 22, 1261.
(62) Schmidt, G. F.; Stuart, H. A. Z. Naturforsch. 1958, 13A, 222.
(63) Itoh, T. Jpn. J. Appl. Phys. 1976, 15, 2295.
(64) Tonelli, A. E. J. Polym. Sci., Polym. Phys. Ed. 1977, 15, 2051.
(65) Wendoloski, J. J.; Gardner, K. H.; Hirschinger, J.; Miura, H.; English, A. D. Science 1990, 247, 431.
(66) Starkweather, H. W., Jr. Macromolecules 1989, 22, 2000.
(67) Harris, D. O.; Engerholm, G. G.; Gwinn, W. D. J. Chem. Phys. 1965, 43, 1515.
(68) Bevington, P. R. Data Reduction and Error Analysis for the Physical Sciences; McGraw-Hill: New York, 1969.
(69) Moore, W. J. Physical Chemistry, 4th ed.; Prentice-Hall: Englewood Cliffs, NJ, 1972; p 622.

Registry No. Nylon 66, 32131-17-2.

Segmental Dynamics in the Amorphous Phase of Nylon 66: Solid-State ^2H NMR†

H. Miura,‡ J. Hirschinger,§ and A. D. English*

Central Research and Development Department, Experimental Station, E. I. du Pont de Nemours and Co., Wilmington, Delaware 19880-0356.
Received August 10, 1989; Revised Manuscript Received October 20, 1989

ABSTRACT: Solid-state deuterium NMR spectroscopy coupled with line shape simulations has been used to examine the segmental dynamics of individual methylene sites and N–D sites within the amorphous domains of selectively deuterated nylon 66 polymers over a wide temperature range. Magnetization only from amorphous domains may be isolated via spin–lattice relaxation time discrimination due to the presence of small-angle fluctuations (librations) at all sites within the amorphous domains above −50 °C. The N–D sites exhibit very little motion below T_g, and above T_g a fraction of the sites undergo nearly isotropic motion. The C–D sites exist in two discrete environments below T_g (*not a continuous distribution*): one of the populations exhibits only librational motion and the other exhibits both librational and internal rotation (γ-relaxation) motions. Above T_g, a fraction of the C–D sites undergo nearly isotropic motion (essentially the same fraction as the N–D sites), and this behavior of the entire repeat unit is identified with the α relaxation. The addition of 2 ± 0.3 wt % water has no apparent effect upon the γ relaxation and depresses the α process by approximately 40 °C; additionally, T_2 relaxation data indicate that the β relaxation is a process which involves all C–D sites and is observed only in wet polymer.

Introduction

In the previous paper in this issue,[1] the dynamics of each chemically distinct methylene group (C–D) and the N–D bond in the amide linkage located within crystalline domains of nylon 66 have been characterized over a wide temperature range with ^2H NMR methods. In the present paper, the analysis of data which is attributable to specific noncrystalline or amorphous domains is described. The molecular motions observed with these methods in various portions of the repeat unit located within crystalline domains are not associated with any of the previously observed mechanical or dielectric relax-

* To whom correspondence should be addressed.
† Contribution No. 5250.
‡ Permanent address: Sumitomo Chemical Co., Tsukuba Research Laboratory, 6 Kitahara, Tsukuba, Ibaraki 300-32, Japan.
§ Current address: Max-Planck-Institut fur Polymerforschung, Postfach 3148, D-6500 Mainz, Federal Republic of Germany.

0024-9297/90/2223-2169$02.50/0